Catchment transit time variability with different SAS function parameterizations for the unsaturated zone and groundwater

Hatice Türk[1], Christine Stumpp[1], Markus Hrachowitz[2], Peter Strauss[3], Günter Blöschl[4], and Michael Stockinger[1]

[1]BOKU University, Institute of Soil Physics and Rural Water Management, Department of Landscape, Water and Infrastructure, Muthgasse 18, 1190 Vienna, Austria
[2]Department of Water Management, Faculty of Civil Engineering and Geosciences, Delft University of Technology, Stevinweg 1, 2628 CN Delft, the Netherlands
[3]Institute for Land and Water Management Research, Federal Agency for Water Management, Petzenkirchen, Austria
[4]Vienna University of Technology, Institute of Hydraulic Engineering and Water Resources Management, Karlsplatz 13, 1040 Vienna, Austria

Correspondence: Hatice Türk (hatice.tuerk@boku.ac.at)

Abstract. Preferential flow paths in hydrological systems (e.g., macropores or subsurface pipe networks) facilitate the rapid transmission of precipitation and solutes to streams, resulting in streamflow responses characterized by the release of young water (i.e., recent precipitation) from the catchment and correspondingly short transit times (on the order of days). While preferential flow paths are documented in both the unsaturated zone and groundwater, it remains uncertain whether catchment-scale isotope-based transport models can adequately represent preferential flow using tracer measurements in streamflow. In this study, we hypothesized that the preferential release of young water from both the unsaturated zone and groundwater contributes measurably to the streamflow tracer signal. This effect can be represented through StorAge Selection (SAS) functions, which specify how young or old water leaves a storage. We systematically compared multiple parameterizations of the SAS functions for the unsaturated zone and groundwater within a single catchment-scale transport model using long-term measurements of hydrogen isotopes in water (δ^2H) from two headwater catchments (the Hydrological Open Air Laboratory (HOAL) in Austria and the Wüstebach catchment in Germany). The results indicated that δ^2H measurements in streamflow exhibited sufficient variability to confirm the preferential release of young water through preferential flow paths in the unsaturated zone. This interpretation was supported by Spearman rank correlations (r) between simulated and observed δ^2H signals in streamflow, where r values ranged from 0.58 to -0.18 for the HOAL catchment and from 0.58 to 0.28 for the Wüstebach catchment, corresponding to SAS shape parameters that reflected a transition from a strong young-water preference to an old-water preference. However, contrary to the unsaturated zone, the variability of δ^2H in streamflow was not sufficient to confirm the prefential release of young water from groundwater storage, as any seasonal variation of δ^2H in pore water was largely dampened by the catchments' substantial passive groundwater storage volumes, with r values ranging between 0.54 and 0.60 in the HOAL, and ranging between 0.71 and 0.76 in the Wüstebach catchment. This interpretation was further supported by the fact that the observed attenuated δ^2H signal in streamflow could only be reproduced when the volume ratio between active and passive groundwater storage was less than 1 %, highlighting the dependence of SAS-based age selection on storage configuration. The damping effect, in combination with the groundwater SAS function parameterization, influenced the estimation of the longer

tails ($100 < T < 1000$ days) of the transit time distributions, making it challenging to quantify how much of the stream water is actually older than 100 days. The variability in streamflow TTD estimates arising from different groundwater SAS function shapes was considerable ($\pm 20\,\%$ for HOAL and $\pm 23\,\%$ for Wüstebach), highlighting that TTD estimates are sensitive to how SAS functions are conceptualized and parameterized within the model. These findings underscore the need for complementary data sources, such as multiple tracers, high-frequency tracer analysis, and/or groundwater-level monitoring, to better constrain preferential flow processes and to reduce uncertainty in catchment-scale water transit time modelling.

1 Introduction

Groundwater plays a crucial role in the hydrological cycle and in sustaining streamflow during low-flow periods, and influences the stream water age and quality (van der Velde et al., 2011; Hamilton, 2012; Kaandorp et al., 2018b). The movement of precipitation through the soil matrix into the groundwater and eventually to the stream spans a wide range of timescales: from rapid responses over days to months (Kaandorp et al., 2018a) to slower contributions over years to decades (Visser et al., 2009; Stewart and Morgenstern, 2016; Wang et al., 2025). The variation in flow timescales across catchments is driven by many factors, including catchment topology and subsurface flow path heterogeneity, which, in turn, leads to spatial and temporal variability in stream water sources and chemical composition (McGuire and McDonnell, 2006; Hamilton, 2012; Kaandorp et al., 2018b). In light of these complexities, previous studies have long underscored that preferential flow pathways in both partially (Beven and Germann, 1982; Weiler et al., 2003; Klaus et al., 2013) and fully saturated porous media (Bianchi et al., 2011) lead to fast and localised water flow and solute transport, which have the potential to alter stream chemical composition. Such preferential flow is widely acknowledged in groundwater hydrology (Berkowitz et al., 2006; Hansen and Berkowitz, 2020a; Berkowitz and Zehe, 2020; Hansen and Berkowitz, 2020b; Zehe et al., 2021), and typically referred to as "non-Fickian" or "anomalous" flow in the groundwater community (Berkowitz and Zehe, 2020; Hansen and Berkowitz, 2020a). While explicitly represented in many dedicated groundwater models (e.g. Berkowitz and Zehe 2020), it remains uncertain whether simpler, top-down catchment-scale, isotope-based transport models can meaningfully represent preferential groundwater flow.

Water molecules entering at different locations within a catchment travel along distinct flow paths and take different times to exit the catchment via streamflow or evaporation (transit time, TT). The statistical distribution of transit times is referred to as the transit time distribution (TTD). The transit time of water reflects the key information about how quickly water moves through a control volume, such as catchments (Beven, 2006; Rinaldo et al., 2015; Benettin and Bertuzzo, 2018); hence, how quickly solutes are transported through the surface, subsurface, and eventually to the stream. Despite their usefulness in studying water flow through catchments, TTs cannot be measured directly and are generally inferred using hydrologic models and catchment-wide input-output signals of tracers, such as water stable isotopes (δ^2H, δ^{18}O). Many studies have integrated hydrometeorological data and applied tracer-based modelling, using the TTD to infer flow processes and estimate transit times (e.g., Birkel et al. 2011a; Kuppel et al. 2018; Benettin and Bertuzzo 2018; Harman 2019; Wang et al. 2023). These studies have shown that streamflow typically consists of water from a broad spectrum of ages, with TTDs spanning from days to

decades, thereby highlighting the importance of both rapid transmission of precipitation to streams and its long-term storage in catchments.

In recent years, studies have focused on time-variable transit time distributions by applying the StorAge Selection (SAS) approach (Botter et al., 2011; van der Velde et al., 2012; Hrachowitz et al., 2016; Harman, 2019), combined with catchment-scale transport models. The SAS function represents water age dynamics in hydrological systems by defining the relationship between the distribution of water ages stored within the system (residence time distribution, RTD) and the distribution of water ages leaving the system as outflows (transit time distribution, TTD). By applying SAS functions with multiple functional forms, such as beta (van der Velde et al., 2015), gamma (Harman, 2019), and piecewise linear (Fenicia et al., 2006; McMillan et al., 2012) distributions, and tracking water fluxes, studies have shown that TTDs vary over time and that transport processes can differ under contrasting conditions, such as between wet and dry periods (Benettin et al., 2015b; Harman, 2015; Kaandorp et al., 2018a). Moreover, using the SAS formulation and conceptualizing the catchment as a multi-bucket system, studies have emphasized the partial age mixing processes of recent precipitation contributing to different fluxes, including evapotranspiration (van der Velde et al., 2015) and macropore flow in the shallow subsurface (Hrachowitz et al., 2013). This preferential flow of precipitation was found to become more prevalent with increasing soil wetness by bypassing smaller pore volumes and releasing younger water (Klaus et al., 2013) or occasionally triggered by high precipitation intensities, leading to overland flow (Türk et al., 2024).

However, despite these findings of partial mixing in the unsaturated zone and the potential of preferential release of young water from groundwater, in many SAS function applications, the age distribution of baseflow (groundwater contribution to streamflow) is simplified by assuming uniform mixing of stored ages (e.g., Benettin et al. 2015a; Birkel et al. 2015; Ala-Aho et al. 2017; Knighton et al. 2019; Hrachowitz et al. 2013, 2021; Salmon-Monviola et al. 2025), noting that SAS functions are not straightforward to parameterize. This simplification is typically adopted i) to maintain model simplicity, ii) due to the lack of robust characterization of subsurface heterogeneity and its induced mixing mechanisms, and iii) due to the limited availability of detailed observations of groundwater flow processes, leaving gaps that must be filled by assumptions such as complete mixing of stored water ages. Nevertheless, several studies have emphasized that TTD estimates depend strongly on the chosen mixing assumptions in SAS models, thereby introducing uncertainty into estimates of transport timescales (van der Velde et al., 2012, 2015; Borriero et al., 2023). Reducing the complexity of groundwater storage representation by employing a single, uniform SAS function shape may, therefore, oversimplify actual groundwater flow processes, potentially leading to erroneous conclusions in the estimation of water transit times.

Indeed, increasing evidence suggests that groundwater systems may not be completely mixed, and that preferential release of young groundwater (e.g, recently recharged water) to streams may be a ubiquitous feature of groundwater in heterogeneous aquifers (Berkowitz and Zehe, 2020; Hansen and Berkowitz, 2020a) for several reasons: (i) time-variant hydrological and climatic conditions (Maxwell et al., 2016), (ii) generally low longitudinal and transversal dispersivities in groundwater systems, leading to little mixing, and (iii) complex structural heterogeneities influenced by geology, soil properties, and land use for very shallow groundwater (Janos et al., 2018). This evidence suggests that groundwater systems are often not completely mixed, and the preferential release of young water may be common in heterogeneous aquifers. Therefore, SAS functions should be

formulated to account for preferential release of young water and the nonlinearities in groundwater contributions and catchment responses.

Furthermore, instead of assuming a single mixed reservoir, and following the conceptualization of Zuber (1986), groundwater is typically described by considering the mixing of active (water that contributes to flow) and passive groundwater storage volumes (water that mixes with the tracer signal of the active water volume but does not contribute directly to flow) (Fenicia et al., 2010; Birkel et al., 2011a; Hrachowitz et al., 2015). Birkel et al. (2011a) emphasised that the presence and extent of the passive storage can significantly influence the interpretation of tracer signals within a catchment. Yet, the extent to which the passive storage volumes and their associated mixing assumptions shape tracer signals and TTD estimations, particularly when combined with different SAS assumptions (e.g., complete mixing vs. partial mixing), still remains to some extent unknown. However, adopting more complex SAS parameterisations with additional parameters may exacerbate model uncertainty, particularly given the limited availability of tracer data to constrain these parameters (Beven, 2006). Consequently, systematically testing different groundwater SAS shapes against long-term tracer observations in streamflow is critical for assessing whether explicitly representing preferential groundwater flow (and associated SAS functions) meaningfully affects the quantification of transit time distributions in catchment-scale isotope-based transport models.

The objective of this study was to test whether stable water isotope (δ^2H) measurements in streamflow can be used within a simple, top-down, catchment-scale transport modeling framework to represent preferential flow in the unsaturated root zone and groundwater, and to assess their influence on transit time distributions. To this end, we evaluated how different parameterizations of SAS functions, which describe the release of younger versus older water from storage, affect simulated tracer signals at the stream outlet. By systematically comparing multiple parameterizations of SAS functions, we tested the hypothesis that the preferential release of young groundwater contributes measurably to the streamflow tracer signal and should therefore be represented in catchment-scale transport models. Additionally, we examined whether (and how) the extent and mixing assumptions of passive groundwater storage influence the interpretation of tracer signals and the estimation of transit times.

We specifically addressed the following research questions:

1. *Do precipitation and stream water tracer data have sufficient variability to identify and characterize preferential groundwater flow processes using different SAS function shapes, and if so, which SAS functions best represent these processes at the catchment scale?*

2. *Does explicitly accounting for the preferential release of young water in groundwater, through a SAS function, affect catchment-scale transit time distributions and simulated tracer signals in streamflow?*

3. *How and to what extent do different groundwater mixing assumptions, in combination with varying passive storage volumes, affect the model's ability to reproduce streamflow tracer signals, and the estimation of transit time distributions at the catchment scale?*

To answer these questions, we used long-term hydrological and δ^2H data from two contrasting headwater catchments. Each site exhibits distinct seasonal variability in streamflow δ^2H signatures: one catchment displays minor isotopic variations during

baseflow and sharp event-based responses (a "flashy" catchment), while the other catchment exhibits pronounced isotopic seasonality even during baseflow conditions. We implemented a time-variant TTD modelling framework capable of representing various mixing scenarios within these catchments.

2 Materials and methods

2.1 Study sites

The study sites for this study were the Hydrological Open Air Laboratory (HOAL) in Petzenkirchen (Fig. S 2), Lower Austria (Blöschl et al., 2016), and the Wüstebach headwater catchment (Fig. S 1) in Germany's Eifel National Park (Bogena et al., 2015). The HOAL covers 66 hectares and features a humid climate with a mean annual air temperature of around 9.5°C. The mean annual precipitation and runoff are approximately 823 $mm\,\mathrm{yr}^{-1}$ and 195 $mm\,\mathrm{yr}^{-1}$, respectively. The elevation ranges from 268 to 323 m a.s.l., with a mean slope of 8 %. Predominant soil types in the HOAL catchment include Cambisols (57 %), Planosols (21 %), Kolluvisols (16 %), and Gleysols (6 %). The area's geology consists of Tertiary fine sediments of the Molasse underlain by fractured siltstone. Land use primarily includes agriculture (commonly maize, winter wheat, and rapeseed) (87 %), supplemented by forest (6 %), pasture (5 %), and paved areas (2 %) (Blöschl et al., 2016).

The Wüstebach headwater catchment, part of the Lower Rhine/Eifel Observatory within the TERENO network, covers 38.5 hectares. It is characterized by a humid climate, with an annual temperature of around 7°C, mean annual precipitation of about 1200 $mm\ \mathrm{yr}^{-1}$, and mean annual runoff of 700 $mm\ \mathrm{yr}^{-1}$. The catchment's elevation ranges from 595 to 630 m a.s.l., with gentle hill slopes surrounding a relatively flat riparian area near the stream. The bedrock is primarily Devonian shales, interspersed with sandstone inclusions and overlaid by periglacial layers. The hillslopes predominantly comprise Cambisols, while the riparian area features Gleysols and Histosols. The land use is primarily spruce forest (Bogena et al., 2018).

2.2 Hydrological and tracer data

We used daily hydro-meteorological data from October 2013 to 2019 for the HOAL catchment (Fig. 1a, 1b) and from October 2009 to October 2013, for the Wüstebach catchment (Fig. 1c, 1d). For the Wüstebach catchment, partial deforestation in October 2013 led to changes in streamflow generation processes (Hrachowitz et al., 2021). Therefore, the period after deforestation was not used for the analyses.

In the HOAL, precipitation data were recorded using a weighing rain gauge located 200 m from the catchment outlet, and stream discharge was measured at the catchment outlet using a calibrated H-flume. The precipitation samples for isotopic analysis were collected using an adapted Manning S-4040 automatic sampler located approximately 300 m south of the catchment. In addition to precipitation samples, weekly grab samples of streamflow were collected at the catchment outlet for isotopic analysis. Additionally, event-based streamflow samples were collected using an automatic sampler, with the frequency of sampling adjusted based on flow rate thresholds (without exceeding sampling bottle capacity). Isotopic measurements of $\delta^{18}\mathrm{O}$ and

δ^2H were conducted using cavity ring-down spectroscopy (Picarro L2130-i and L2140-i), with an analytical uncertainty of ± 0.1 ‰ for δ^{18}O and ± 1.0 ‰ for δ^2H.

In the Wüstebach catchment, precipitation data were obtained from a nearby meteorological station operated by the German Weather Service (Deutscher Wetterdienst, DWD station 3339), and stream discharge was measured using a V-notch weir for low flows and a Parshall flume for high flows (Bogena et al., 2015). The precipitation samples for isotopic analysis were collected at the Schöneseiffen meteorological station, located approximately 3 km northeast of the catchment at an elevation of 620 m a.s.l. Starting in June 2009, weekly precipitation samples were collected using a cooled storage rain gauge with 2.3-L HDPE bottles (Stockinger et al., 2014). From September 2012 onward, the sampling resolution was increased to daily intervals (Fig. 1d) using a cooled automated sampler (Eigenbrodt GmbH & Co. KG, Germany; 250 mL PE bottles). Stream water samples for isotopic analysis were collected weekly at the catchment outlet as grab samples. Cavity ring-down spectroscopy (Picarro L2120-i, L2130-i) was used for water isotope analyses, with an analytical uncertainty of ± 0.1 ‰ for δ^{18}O and ± 1.0 ‰ for δ^2H. All isotopic measurements are reported as per mil (‰) relative to Vienna Standard Mean Ocean Water (VSMOW).

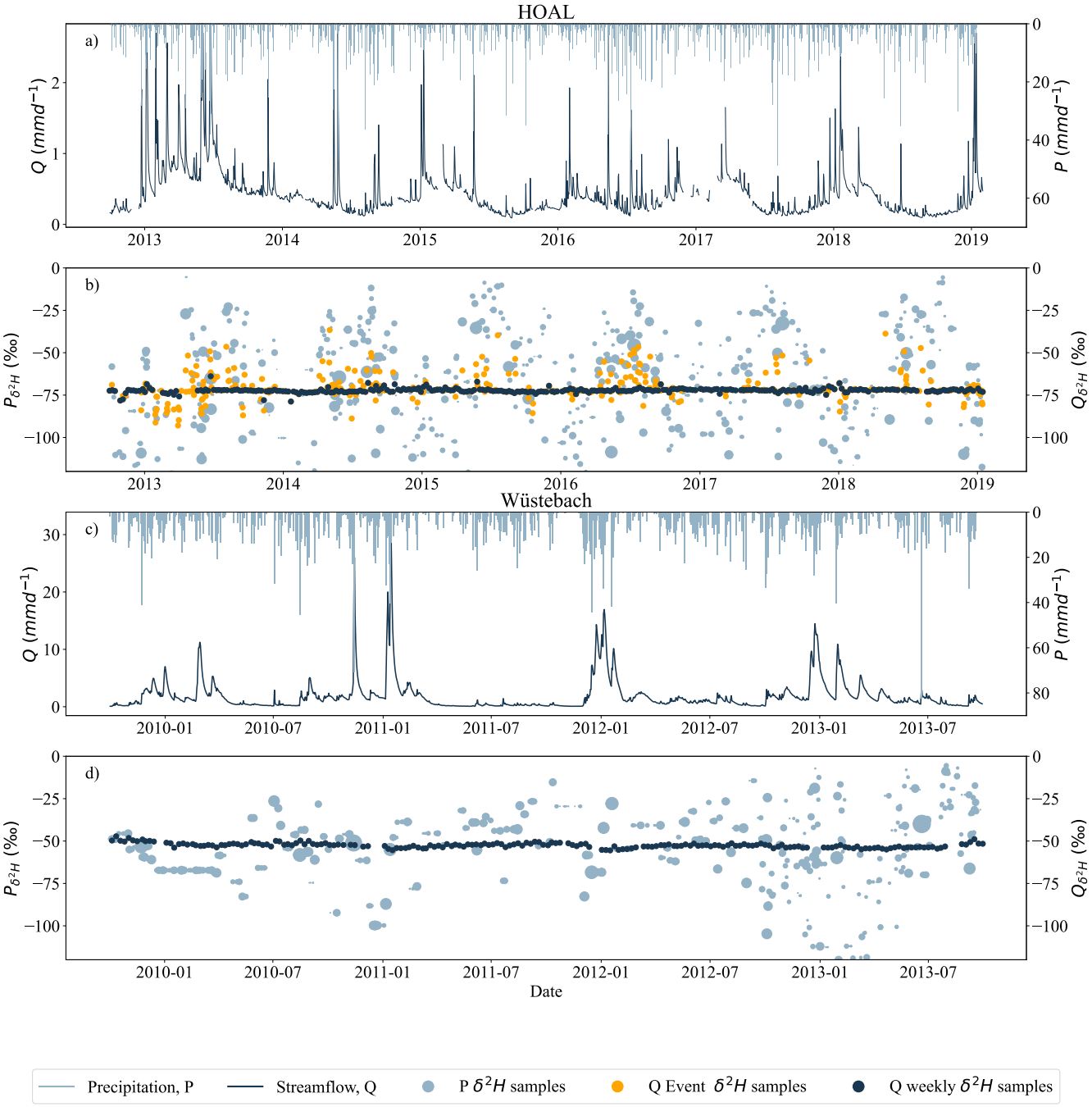

Figure 1. Hydrological and tracer data of the HOAL and Wüstebach catchments. (a, c) daily measured streamflow Q (mmd^{-1}) and precipitation P (mmd^{-1}), (b, d) precipitation δ^2H signals (light blue) and streamflow δ^2H signals (dark blue); the size of the dots indicates the relative precipitation volume. For the HOAL catchment, the δ^2H data of streamflow was further shown as the weekly grab samples (b, dark blue dots) and event samples (b, orange dots). For the HOAL catchment, precipitation δ^2H samples are in daily resolution, whereas for the Wüstebach catchment, beginning in September 2012, the sampling frequency for precipitation δ^2H increased from weekly to daily (d).

2.3 Hydrological model and tracer transport model

We used a process-based hydrological and transport model (Türk et al., 2024) based on the DYNAMITE modelling framework (Hrachowitz et al., 2014). Briefly, both the HOAL and Wüstebach catchments are conceptualised through five interconnected reservoirs: snow, canopy interception, unsaturated root zone, fast response storage, and groundwater with active and passive components (Fig. 2). The model hydrological fluxes are: total precipitation P (mm d^{-1}), precipitation as snow P_s (mm d^{-1}), precipitation as rain P_r (mm d^{-1}), snow-melt P_m (mm d^{-1}), throughfall P_e (mm d^{-1}), interception evaporation E_i (mm d^{-1}), evaporation from the root zone E_a (mm d^{-1}), preferential fast response R_f (mm d^{-1}), fast preferential recharge to the to groundwater R_{fs} (mm d^{-1}, preferential fast response R_{ff} (mm d^{-1}), infiltration-excess overland flow Q_o (mm d^{-1}), preferential fast response to the fast-responding bucket R_{fn} (mm d^{-1}), flow from the fast-responding reservoir Q_f (mm d^{-1}), saturation-excess overland flow from the fast-response bucket Q_{of} (mm d^{-1}), slow recharge to the groundwater reservoir R_s (mm d^{-1}), baseflow from the groundwater reservoir Q_s (mm d^{-1}), deep infiltration loss Q_l (mm d^{-1}), and the total discharge to the streamflow Q_{tot} (mm d^{-1}). Model calibration parameters are shown in red adjacent to the model component they are associated with (Fig. 2), and symbols are defined in Table S 2. All model equations are defined in Table S 1

To route δ^2H fluxes through the model, the SAS approach (Rinaldo et al., 2015; Harman, 2015) was integrated into the hydrological model. In this integrated framework, each storage defined within the hydrological model (e.g., S_r, S_f, Fig. 2), at any given time t, stores water of different ages, represented as T, which traces back to past precipitation and is ranked by their input time. The age distribution of a storage at time t is termed $p_s(T,t)$, and is in its cumulative form $S_T(T,t)$, also known as the cumulative residence time distribution (RTD). The output fluxes O (mm d^{-1}) (e.g., E_a, R_s, Fig. 2) are subsets of specific ages from the storage with water age distributions termed $p_{Q,T}(T,t)$, which are known in their respective cumulative form $O_T(T,t)$ as cumulative transit time distributions (TTD). The relation between storage and output fluxes is formulated based on the SAS function $\omega_{O,m,j}$ that SAS defines the likelihood of selecting water parcels of different ages for release from the storage, thereby translating the internal age structure of the storage into an age distribution of output fluxes. At each time t, the age-ranked water in storage is characterized by its tracer composition $C_S(T,t)$, which reflects the signal of past precipitation inputs. The output fluxes are likewise described by their tracer distributions, $C_O(T,t)$, derived from the selection of water ages leaving storage.

Then, the transport balance of the storage is built on water age conservation over time :

$$\frac{\partial S_{T,j}(T,t)}{\partial t} + \frac{\partial S_{T,j}(T,t)}{\partial T} = \sum_{n=1}^{N} I_{T,n,j}(T,t) - \sum_{m=1}^{M} O_{T,m,j}(T,t) \tag{1}$$

where: $\frac{\partial S_T(T,t)}{\partial t}$ is the rate of change of age-ranked storage with respect to time, $\frac{\partial S_T(T,t)}{\partial T}$ represents the ageing of water within the storage, $I_{T,n}(T,t)$ are the cumulative age-ranked inflows $O_{T,m,j}(T,t)$ are the cumulative age-ranked outflows. N and M denote the number of inflows and outflows from a given storage component (e.g., for the root zone, N would be P_e and M is E_a, R_f, and R_s; see Fig.2). Each age-ranked outflow $O_{T,m,j}(T,t)$ (Eq.2) from a specific storage component j depends on the cumulative age distribution of that outflow $P_{O,m,j}(T,t)$ and outflow volume $O_{m,j}(t)$, which is estimated by the hydrological

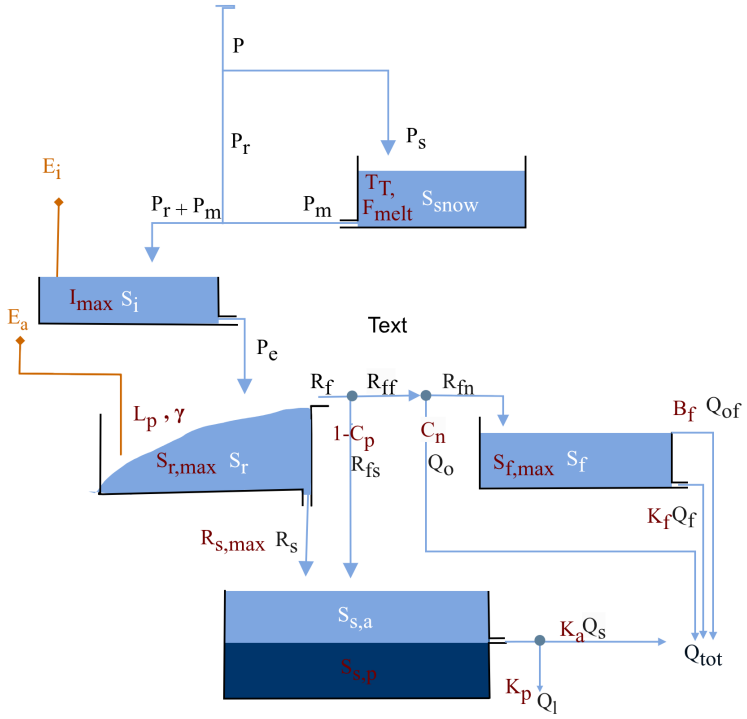

Figure 2. The model structure used to represent the HOAL and the Wüstebach catchment (adapted from Türk et al. (2024)). Light blue boxes indicate the hydrologically active storage volumes that contribute to total discharge Q_{tot}: Snow storage (S_{snow}), canopy interception (S_i), fast response bucket (S_f), root zone storage (S_r), and "active" groundwater ($S_{s,a}$). The darker blue box ($S_{s,p}$) indicates a hydrologically "passive" groundwater volume. Blue lines indicate snow and water fluxes, while orange lines indicate water vapour fluxes. Model parameters are shown in red adjacent to the model component they are associated with and symbols are defined in Table S 2. All model equations are defined in Table S 1

balance component of the model.

$$O_{T,m,j}(T,t) = O_{m,j}(t)\, P_{O,m,j}(T,t), \tag{2}$$

where $O_{m,j}(t)$ is the total outflow rate, and

$$P_{O,m,j}(T,t) = \Omega_{o,m,j}\big(S_{T,j}(T,t), t\big) \tag{3}$$

The cumulative age distribution $P_{O,m,j}(T,t)$ (Eq.3) is the backward TTD of that outflow in cumulative form and depends on the age-ranked distribution of water in the storage component j at time t, $S_{T,j}(T,t)$, and the probability density function, which in this case is the SAS function $\omega_{O,m,j}$ (or $O_T(T,t)$ in its cumulative form) of that flux.
From the cumulative age distribution, the associated probability density function can be derived according to

$$p_{o,m,j}(T,t) \;=\; \overline{\omega}_{o,m,j}\big(S_{T,j}(T,t),t\big)\,\frac{\partial S_{T,j}(T,t)}{\partial T}\,, \tag{4}$$

where $\omega_{o,m,j}(S,t)$ is a probability density function of normalized rank storage $S_{T,\mathrm{norm},j}(T,t)$ (Eq. 5). Normalizing the age-ranked storage $S_T(T,t)$ by its total volume $S_j(t)$ binds $S_{T,\mathrm{norm},j}$ to the interval $[0,1]$ and holds mass balance without requiring rescaling of the SAS function at each time step.

$$S_{T,\mathrm{norm},j}(T,t) \;=\; \frac{S_{T,j}(T,t)}{S_j(t)}\,, \tag{5}$$

so that $0 \leq S_{T,\mathrm{norm},j} \leq 1$.

Finally, the tracer composition of outflow m from compartment j is computed as :

$$C_{O,m,j}(t) \;=\; \int_0^{S_j} C_{S,j}\big(S_{T,j}(T,t),t\big)\,\overline{\omega}_{O,m,j}\big(S_{T,j}(T,t),t\big)\,\mathrm{d}S_T \tag{6}$$

where $C_{O,m,j}(t)$ is the tracer composition in outflow m from storage component j at time t, and $C_{S,j}$ is the tracer composition in storage at time t. The model reproduces TTDs for all fluxes and storage components (Fig. 2) at each time step t. Further details on the model architecture and assumptions can be found in previous studies (Hrachowitz et al., 2014; Fovet et al., 2015). The water balance and flux equations for the two catchments in this study application are described in Türk et al. (2024) and provided in the supplementary Table S 1

Similar to previous tracer transport studies for the HOAL (Türk et al., 2024) and Wüstebach (Hrachowitz et al., 2021) catchments, we used beta distributions to formulate the SAS functions. Beta distributions are defined by two shape parameters (α and β). When both parameters of the Beta distribution were equal to 1 ($\alpha = \beta = 1$), water is uniformly sampled from storage without any preference for specific ages. If $\alpha < \beta$ (or $\alpha > \beta$), a selection preference for younger (or older) water existed, respectively. To limit the number of model parameters, β was fixed at 1. The time variability of the SAS function shape was then determined by the age-ranked storage and the shape parameter α, which was bounded between 0 and 1 to represent a preference for younger storage, and greater than 1 to represent a preference for older storage. Preferential release of older water ($\alpha > 1$) decreases the mean residence time of stored water, as older water is removed from storage. Conversely, preferential release of younger water ($\alpha < 1$) increases the mean residence time of stored water, as older water remains stored for longer periods.

In principle, the model has 16 outfluxes (Fig. 2), and each of the outflux (e.g., E_a, R_s) requires a separate SAS function parameter α to be calibrated. However, this is computationally infeasible and would introduce model parameter complexity. Therefore, for all modelled outflows, α and β were fixed at 1, except those representing preferential flow from the unsaturated root zone (named as $S_{U,alpha}$ Table S 2), the α and β parameters were fixed at 1 for model calibration.

In the Wüstebach catchment, previous studies (Wiekenkamp et al., 2016; Hrachowitz et al., 2021) showed that catchment soil wetness is the main driver for activating preferential flow pathways in the unsaturated zone, leading to the preferential release of young water to the streamflow as soil wetness increases. Therefore, the SAS function shape parameter representing

preferential flow from the unsaturated root zone (R_f, Fig. 2) was formulated as a time-variable function of relative soil wetness ($S_r/S_{r,\max}$), where S_r is the water volume in the root zone at time t, and $S_{r,\max}$ is the maximum root-zone storage capacity (calibrated parameter). Equation 8 adopts an increasing probability of young water release with increasing soil wetness through the time-dependent shape parameter $\alpha(t)$, reflecting changes in transport processes between wet and dry soil conditions.

In the HOAL catchment, previous studies have highlighted the non-linearity of preferential flow generation in the unsaturated zone, where both precipitation intensity and soil wetness control the activation of preferential flow pathways (Széles et al., 2020; Vreugdenhil et al., 2022). Overland flow occurs when precipitation exceeds a certain threshold, routing recent precipitation directly to the stream with minimal interaction with stored water (Türk et al., 2024). To account for the combined roles of soil wetness and precipitation intensity in the activation of preferential flow and the release of young water in HOAL catchment, we parameterized the SAS function for preferential flow from the unsaturated root zone (R_f, Fig. 2) using a time-variable shape parameter $\alpha(t)$ defined as a function of both soil wetness state and precipitation intensity. Specifically, $\alpha(t)$ was formulated as a function of relative soil wetness (scaled by the maximum root-zone storage capacity, $S_{r,\max}$) and precipitation intensity (P_I, $\mathrm{mm\,d^{-1}}$), with a threshold parameter (P_{thresh}) controlling the onset of precipitation-driven preferential flow. This causal formulation was implemented to ensure that $\alpha(t)$ dynamically responds to both wetness conditions and event-scale precipitation forcing, allowing the model to capture the non-linear activation of preferential flow observed in the catchment. The dual dependence of $\alpha(t)$ on soil wetness and precipitation intensity, therefore, extends previous SAS applications by providing a more flexible representation of unsaturated zone preferential flow dynamics in HOAL.

For the HOAL catchment, the time variability of α for preferential flow in the unsaturated root zone was defined as:

$$\alpha(t) = \begin{cases} \alpha_0, & \text{if } P_r(t) \geq P_{\mathrm{thresh}} \\ 1 - \frac{S_r(t)}{S_{r,\max}}(1-\alpha_0), & \text{if } P_r(t) < P_{\mathrm{thresh}} \end{cases} \tag{7}$$

For the Wüstebach catchment, time variability of α for the preferential flow in the unsaturated root zone was defined as:

$$\alpha(t) = 1 - \left(\frac{S_r(t)}{S_{r,\max}}\right)(1-\alpha_0) \tag{8}$$

In both Equations 7 and 8, the time variable shape parameter $\alpha(t)$ controls the preferential release of younger water: values of $0 < \alpha(t) < 1$ indicate a bias towards younger water parcels, whereas $\alpha(t) = 1$ corresponds to uniform sampling. The α_0 is a calibration parameter representing the lower bound between 0 and 1, allowing $\alpha(t)$ to vary between α_0 and 1. When soil wetness is low ($S_r(t) \ll S_{r,\max}$), $\alpha(t)$ approaches 1, indicating uniform sampling. As soil wetness increases ($S_r(t)$ approaches $S_{r,\max}$), $\alpha(t)$ decreases towards α_0, reflecting a stronger preference for younger water. In Equation 7, the lower bound α_0 is applied directly whenever precipitation intensity exceeds a certain threshold (P_{thresh}).

2.3.1 Model calibration and evaluation

We used daily time steps in the model parameter calibration for the period from October 2014 to 2019 for the HOAL catchment and for the period from October 2010 to October 2013 for the Wüstebach catchment to simulate streamflow Q ($mm\,\mathrm{d^{-1}}$) and

δ^2H signature. The model warm-up period was one year for both catchments; i.e., from October 2013 to October 2014 for the HOAL catchment, and from October 2009 to October 2010 for the Wüstebach catchment.

For model parameter optimization, we used the Differential Evolution algorithm (Storn and Price, 1997) and an objective function that combined five performance criteria related to streamflow and δ^2H dynamics. The objective function included the Nash-Sutcliffe efficiencies (NSE) of streamflow (to evaluate overall discharge dynamics), logarithmic streamflow (to match low-flow conditions), the flow duration curve (to capture the distribution of flows over time), the runoff coefficient averaged over three months (to ensure water balance consistency), and the NSE of the δ^2H signal in streamflow (to constrain δ^2H dynamics) (Table S 3). These individual performance metrics were aggregated into the Euclidean distance D_E, with equal weights assigned to streamflow and the δ^2H signature, according to:

$$D_E = \sqrt{\frac{1}{2}\left(\frac{\sum_{i=m}^{M}(1-E_{Q,m})^2}{M} + \frac{\sum_{i=n}^{N}(1-E_{18O,n})^2}{N}\right)} \tag{9}$$

Where $M = 4$ is the number of performance metrics with respect to streamflow, $N = 1$ is the number of performance metrics for tracers, and E is the evaluation matrix based on goodness-of-fit criteria. The Euclidean distance D_E to the "optimal model" (where $D_E = 0$ indicates a perfect fit) was used to ensure that overall model performance remained balanced. Only solutions achieving $D_E \leq 1$ were accepted as feasible solutions for further analysis. The accepted solutions were then ranked in order of decreasing D_E, and the solution with the lowest D_E was selected as the parameter set for TTD estimations. Transit times were estimated up to a tracking period of 1000 days, limited by data availability, and the mean of the estimated TTD was compared between dry periods (streamflow below the 25$^{\text{th}}$ percentile, Q_{25}) and wet periods (streamflow above the 75$^{\text{th}}$ percentile, Q_{75}). In addition, the young-water fraction of daily streamflow ($F_{Q(T<90)}$) was calculated as the sum of streamflow fractions with transit times up to 90 days. Its monthly variability was then analyzed in relation to the corresponding monthly variability of soil wetness $\left(\frac{S_r}{S_{r,\max}}\right)$ for both catchments.

2.3.2 Sensitivity test of root zone and groundwater SAS functions

In this analysis, we systematically tested the sensitivity of the streamflow δ^2H signal simulations and inferred transit times to changes in the StorAge Selection (SAS) function parameterization for both the unsaturated root zone and the groundwater compartments. We first tested the sensitivity of the streamflow δ^2H signal to root-zone preferential flow by systematically varying the lower bound of the SAS shape parameter α_0 across four values: 0.1 (very young-water preference), 0.7 (young-water preference), 1.0 (uniform selection), and 5.0 (older-water preference), while keeping the groundwater SAS function uniform (i.e., $\alpha = 1$; Fig. 3a). This approach assesses whether different parametrizations of the SAS function for root-zone preferential pathways alone could reveal a strong impact on the simulated streamflow δ^2H time series and the inferred transit times. Next, we tested the sensitivity of the δ^2H signal to changes in the groundwater SAS function (Fig. 3b) by varying α across the same range—0.1, 0.7, 1.0, and 5.0—while fixing the previously calibrated optimized α_0 value for the root-zone preferential flow. This second test was designed to show if (and how) different parametrizations of the SAS function for groundwater flow

influence the simulated streamflow δ^2H and time series transit time distributions. We evaluated the model's performance in simulating δ^2H using Spearman rank correlation, $\mathrm{NSE}_{\delta^2\mathrm{H}}$, and $\mathrm{MAE}_{\delta^2\mathrm{H}}$. Finally, we calculated daily cumulative TTDs and compared how their means changed across all scenarios to quantify the impact of SAS function shape on modeled water age distributions. It should be noted that the SAS formulation can only indicate whether preferential release of young water occurs. It does not capture the physical processes driving this behavior, such as soil hydraulic properties, macropore flow, or transient groundwater connectivity.

To isolate the effect of the SAS function shape on the simulated streamflow δ^2H signal and on the estimated transit time distributions (TTDs), all hydrological model parameters (e.g., maximum percolation rate, storage capacities, and flow path configurations) were kept identical to the individually calibrated values for the HOAL and Wüstebach catchments. By using the same calibrated parameters while testing different SAS parameterizations for HOAL and Wüstebach, any differences in the simulated δ^2H signals or TTDs can therefore be attributed solely to changes in the SAS function parameterization.

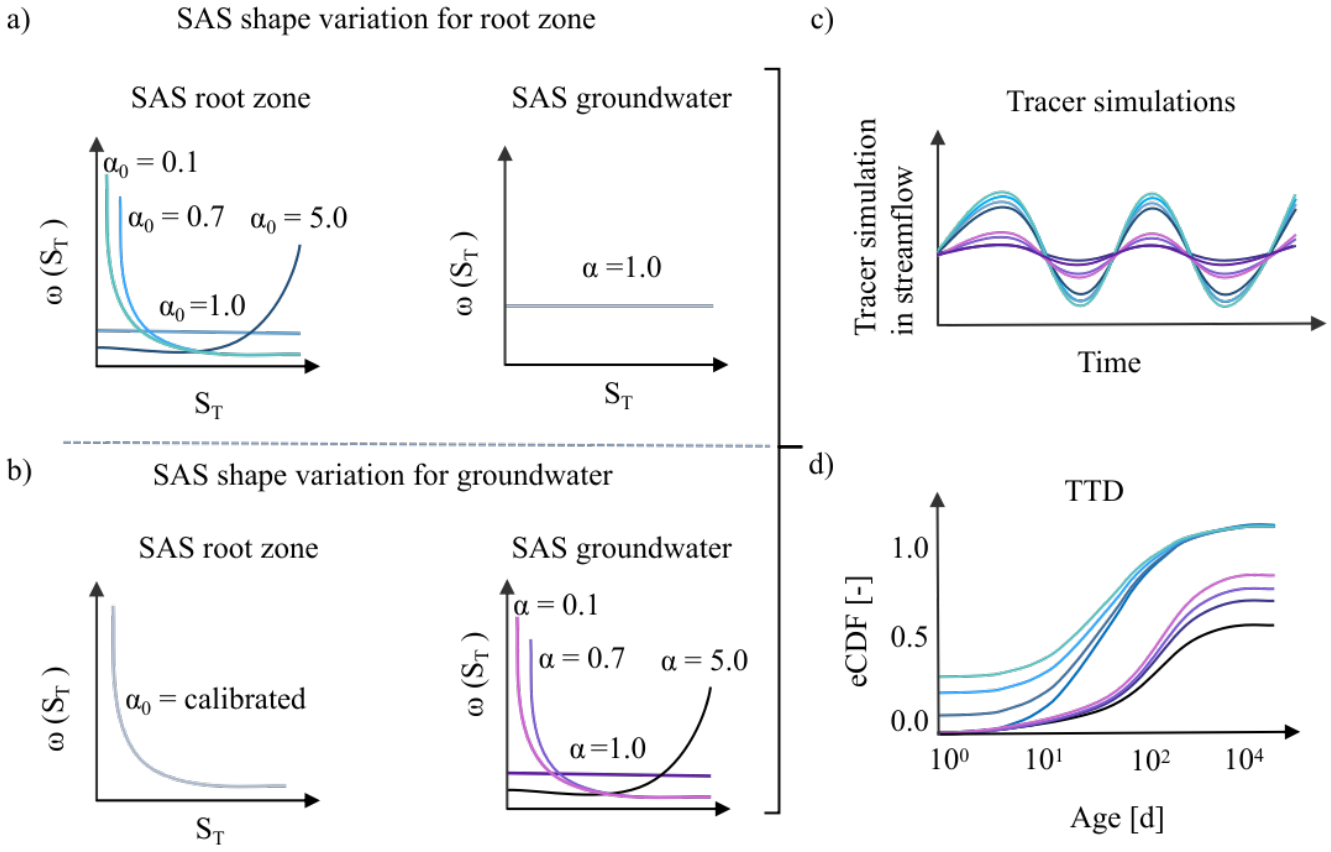

Figure 3. Conceptual representation of the stepwise analysis illustrating how different SAS functions, formulated with the lower bound of the shape parameter α_0 for root-zone preferential flow and α for groundwater flow, affect the simulated tracer signals and inferred transit time distributions (TTDs). (a) The unsaturated root-zone SAS function shape parameter α_0 is varied from 0.1 (strong young-water preference, light blue line) to 5.0 (old-water preference, dark blue line), while the groundwater age selection remains uniform. (b) The root-zone SAS function shape parameter α_0 is fixed at its calibrated value, and the groundwater α is varied from 0.1 (strong young-water preference, light purple line) to 5.0 (old-water preference, dark purple line). (a, b) The x-axis, S_T, represents the age-ranked storage, and the y-axis, $\omega(S_T)$, denotes the relative probability of releasing water of that age. (c, d) Illustrate the modeled tracer time series based on the scenarios implemented in (a) and (b), and the corresponding empirical cumulative transit time distributions.

2.4 Passive groundwater storage volumes and mixing assumptions with the active groundwater storage

In this analysis, we tested whether and to what extent the mixing of the passive groundwater storage with the active groundwater modulates the δ^2H signal in streamflow and, consequently, influences model performance and inferred transit times. We extended the stepwise analysis (Fig. 3b) by varying passive storage volumes (Fig. 4). In the model setup, groundwater storage was represented as an *active* component ($S_{s,a}$) and a hydrologically *passive* component ($S_{s,p}$, mm). The passive storage ($S_{s,p}$) does not contribute to baseflow quantity but isotopically mixes with the water of active storage, as illustrated in Figure 2. For the SAS function, the total groundwater storage was defined as the sum of both components ($S_{s,\mathrm{tot}} = S_{s,a} + S_{s,p}$). Consequently, the age-ranked total groundwater storage ($S_{s,\mathrm{tot}}$) represents the combined influence of active and passive storage on the age composition of baseflow (Q_s, Fig. 2).

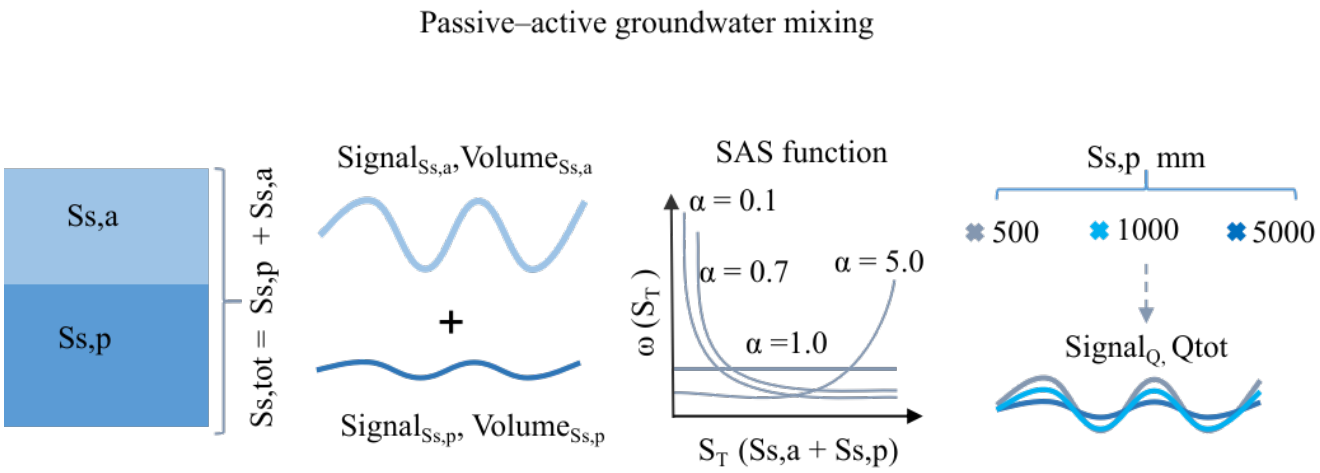

Figure 4. Conceptual representation of the analysis illustrating how different passive storage volumes ($S_{s,p}$ = 500, 1000, and 5000 mm) interact with the active storage volume ($S_{s,a}$) under various groundwater SAS function shapes affecting tracer simulations in streamflow. The groundwater SAS function parameter α is varied from 0.1 (strong young-water preference) to 5.0 (old-water preference). For the SAS function, the x-axis, S_T, represents the age-ranked total groundwater storage, and the y-axis, $\omega(S_T)$, denotes the relative probability of releasing water of that age.

We applied three different passive storage volumes ($S_{s,p} = 500$ mm, 1000 mm, and 5000 mm) to cover the ranges reported for comparable headwater catchments (Birkel et al., 2011a; Benettin et al., 2015a; Hrachowitz et al., 2021). To isolate the effect of passive storage and age-selection parameterization on streamflow δ^2H dynamics and TTD estimations, we kept all hydrological model parameters (e.g., maximum percolation rate, storage capacities, and flow path configurations) identical to the individually calibrated values for the HOAL and Wüstebach catchments. Similar to Figure 3b, four different groundwater SAS parameterizations were tested (Fig. 4): a strong preference for younger water ($\alpha = 0.1$), a preference for younger water ($\alpha = 0.7$), uniform selection ($\alpha = 1.0$), and a preference for older water ($\alpha = 5.0$). We evaluated model performance in simulating streamflow δ^2H by comparing measured and modeled isotope signals using $\mathrm{NSE}_{\delta^2\mathrm{H}}$ and $\mathrm{MAE}_{\delta^2\mathrm{H}}$. In addition, we

calculated daily cumulative TTDs and compared the means of these distributions across different passive storage volumes and SAS parameterizations.

3 Results

3.1 Variation of δ^2H in precipitation and streamflow

In the HOAL catchment, δ^2H values in precipitation ranged from -3.0 ‰ to -150.0 ‰ (Fig. 1b), with a volume-weighted mean of -67.7 ‰ $\pm$ 31.9 ‰. Event-based streamflow δ^2H samples ranged from -26.2 ‰ to -108.0 ‰ (Fig. 1b), while weekly streamflow δ^2H samples ranged from -73.2 ‰ to -75.2‰. The overall volume-weighted mean of stream samples was -71.6 ‰ $\pm$ 6.1 ‰.

In the Wüstebach catchment, δ^2H values in precipitation ranged from -4.3 ‰ to -163.2 ‰ (Fig. 1d, light blue dots), with a volume-weighted mean of -52.2 ‰ $\pm$ 21.4 ‰. Weekly streamflow δ^2H values exhibited smaller variations, ranging from -45.6 ‰ to -57.1 ‰ (Fig. 1d). The volume-weighted mean of stream samples was -53.2 ‰ $\pm$ 1.4 ‰.

Overall, δ^2H in precipitation exhibited large variability in both catchments; however, this signal was attenuated in streamflow. In the HOAL catchment, event-based streamflow δ^2H samples reflected how precipitation inputs were rapidly transmitted to the stream, whereas weekly samples alone would have masked this variability. This highlights the importance of event-based sampling for detecting preferential flow signals, which may remain obscured with weekly data alone. This applies to the Wüstebach catchment, where only weekly streamflow δ^2H measurements were available, which may have prevented the detection of such rapid responses.

3.2 Model calibration

Model calibration resulted in 55 feasible (acceptable model performance with DE < 1) parameter solutions for HOAL (Fig. S 3) and 190 feasible parameter solutions for the Wüstebach catchment (Fig. S 4). The model reproduced the main features of the hydrograph and captured both the timing and magnitude of high and low flow events for the simulation period from October 2014 to 2019 for HOAL (Fig. S 5a, d) and from October 2010 to October 2013 for the Wüstebach catchment (Fig. S 5e, h).

For the HOAL catchment, the mean Nash-Sutcliffe efficiency of streamflow (NSE_Q) for the 55 solutions was 0.60 (Fig. S 6). Minor dissimilarities occurred during the spring of 2016, when low flows were overestimated (Fig. S 5a). Nevertheless, the model simulated most other observed flow signatures reasonably well (Fig. S 6). Among the 55 solutions, the mean NSE for low flows ($\text{NSE}_{\log Q}$) was 0.65, for the flow duration curve (NSE_{FDC}) was 0.53, and for the three-month averaged runoff ratio (NSE_{RC}) it was 0.85. For several rain events, the model captured δ^2H fluctuations during high flows and maintained a stable δ^2H signal during low flows, with a mean $\text{NSE}_{\delta^2\text{H}}$ of 0.51. Overall, the Euclidean distance (D_E) for these 55 solutions ranged from 0.60 to 0.33 (Fig. S 6).

For the Wüstebach catchment, the mean NSE of streamflow (NSE_Q) for the 190 solutions was 0.78 (Fig. S 6). Minor dissimilarities occurred during the spring of 2012, when low flows were overestimated, and the winter of 2012, when peak flows were

underestimated (Fig. S 5e). Among the 190 solutions, the mean NSE for low flows ($\mathrm{NSE}_{\log Q}$) was 0.65, for the flow duration curve ($\mathrm{NSE}_{\mathrm{FDC}}$) it was 0.93, and for the three-month averaged runoff ratio ($\mathrm{NSE}_{\mathrm{RC}}$) it was 0.91. For several rain events, the model captured δ^2H fluctuations during high flows and maintained a stable δ^2H signal during low flows, with a mean $\mathrm{NSE}_{\delta^2\mathrm{H}}$ of 0.58. Overall, the Euclidean distance (D_E) for these 190 solutions ranged from 0.62 to 0.32 (Fig. S 6).

3.3 Modeled catchment transit times

Figure 5 presents the transit time distributions (TTDs) estimated from the initial model calibration, conducted prior to the stepwise experiments. For TTD estimations, we used the model-calibrated parameter set that yielded the lowest D_E. The results presented hereafter are conditional on the underlying model assumptions and should be interpreted in light of the associated uncertainties.

In the HOAL catchment, the fraction of streamflow younger than 1000 days exhibited considerable variability, ranging from 5 % to 50 % (Fig. 5a). The mean fraction of discharge younger than 1000 days was 13 %; it increased to 15 % during wet periods and decreased to 10 % during dry periods (Fig. 5a). The value of the fraction of streamflow younger than 90 days, $\mathrm{F_Q}(T < 90\,\mathrm{days})$, varied widely within the same calendar month, ranging from 2 % to 45 %; however, the mean $\mathrm{F_Q}(T < 90\,\mathrm{days})$ across months did not exhibit pronounced seasonal patterns (Fig. 5b). The mean value of simulated relative soil saturation ($S_r/S_{r,\max}$) varied from 0.25 to 0.60 (Fig. 5c).

In the Wüstebach catchment, the mean fraction of discharge younger than 1000 days was 27 %, increasing to 35 % during wet periods and decreasing to 20 % during dry periods (Fig. 5d). The value of the fraction of streamflow younger than 90 days, $\mathrm{F_Q}(T < 90\,\mathrm{days})$ within the same calendar month ranged between 5 % and 30 % (Fig. 5e), with mean values exhibiting seasonal patterns. The monthly mean of simulated relative soil saturation ($S_r/S_{r,\max}$) ranged from approximately 0.60 to 0.98 (Fig. 5f).

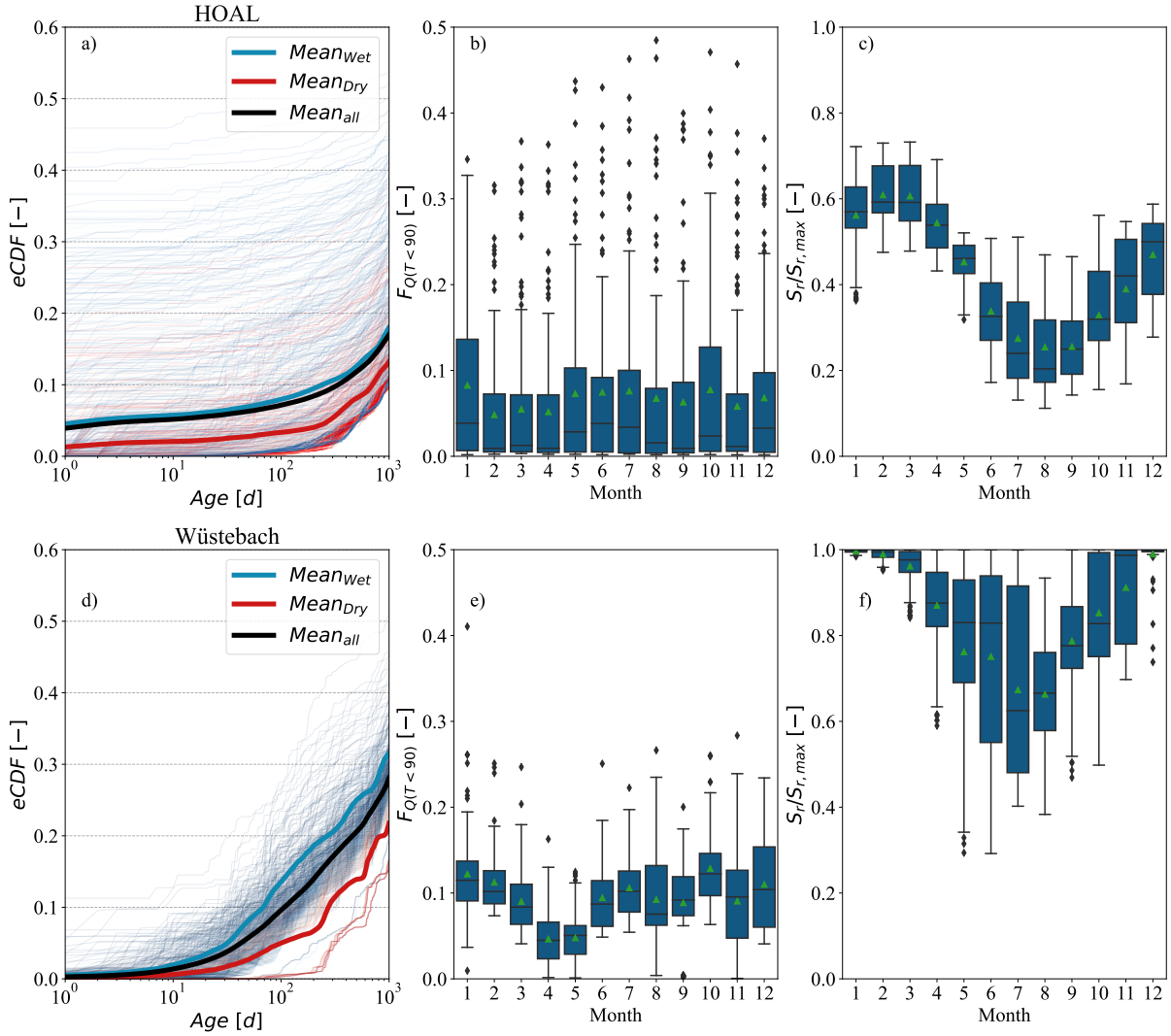

Figure 5. Modelled empirical cumulative transit time distributions (TTDs) for daily streamflow in the (a) HOAL and (d) Wüstebach catchments. The colour of the lines corresponds to the wetness state, where dark blue indicates a wet period and dark red indicates a dry period. In panels (a) and (d), the mean of the empirical cumulative TTDs is shown for the entire tracking period (black line), the dry period (red line), and the wet period (dark blue line). The fraction of streamflow younger than 90 days, $\mathrm{F_Q}(T < 90)$, grouped by month of the year, is shown in panels (b) and (e) for the HOAL and Wüstebach catchments, respectively. Simulated relative soil wetness $\left(\frac{S_r}{S_{r,\max}}\right)$, also grouped by month of the year, is shown in panels (c) and (f) for the HOAL and Wüstebach catchments, respectively. Green triangles in panels b, c, e, and f show the mean values.

3.4 Sensitivity of δ^2H simulations and TTD estimation to different SAS functions in the root zone

In the HOAL catchment, the calibrated root-zone SAS shape parameter lower bound ($\alpha_0 = 0.14$) indicated a strong preference for very young water through unsaturated root-zone preferential flow pathways. These reflected the SAS formulation (Eq. 7) on the dual dependence of $\alpha(t)$ on soil wetness and precipitation intensity. Under high-intensity precipitation, $\alpha(t)$ takes a value of 0.14, indicating that rapid activation of preferential pathways occurs, allowing precipitation inputs to reach the stream with minimal mixing with stored water. In contrast, under wetter antecedent conditions, $\alpha(t)$ increases toward 1, indicating greater mixing within the root zone and contributions of relatively older (i.e., older than recent precipitation inputs) water to streamflow.

In the Wüstebach catchment, the calibrated SAS shape parameter lower bound ($\alpha_0 = 0.98$) suggested only a slight preference for young water. Here, $\alpha(t)$ varied between 0.98 and 1 depending on the soil wetness state (Eq. 8). Under wetter antecedent conditions, established preferential flow pathways facilitated more mixing compared to overland flow, leading to relatively older (i.e., older than recent precipitation) water contributions.

For both catchments, root-zone preferential flow SAS functions ranging from a strong young water preference ($\alpha_0 = 0.1$) to uniform sampling ($\alpha_0 = 1.0$) produced high (positive) Spearman rank correlations (r) between modeled and observed δ^2H. In contrast, an old-water preference ($\alpha_0 = 5.0$) yielded negative or weak correlations, indicating a poor fit to the observed tracer signals. In HOAL, the r values ranged between 0.58, and -0.18 for values of α_0 between 0.1 and 5.0 (Fig. 6a). The corresponding Nash–Sutcliffe efficiencies ($\mathrm{NSE}_{\delta^2\mathrm{H}}$) ranged between 0.56, and -0.25 (Table 1). In Wüstebach, the r values for simulated δ^2H ranged between 0.58, and 0.28 for values of α_0 between 0.1 and 5.0 (Fig. 6b). The corresponding $\mathrm{NSE}_{\delta^2\mathrm{H}}$ ranged beetwe 0.51 and -0.14 (Table 1).

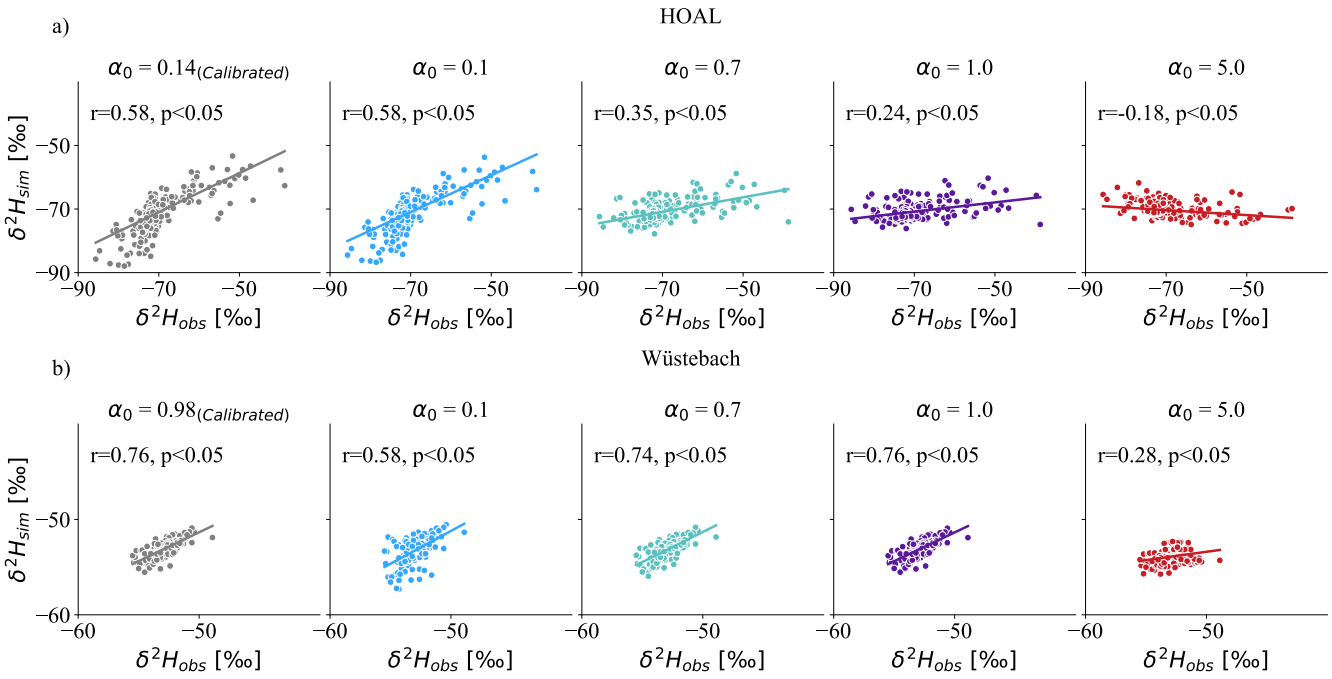

Figure 6. Spearman rank correlations between simulated (y-axis) and observed (x-axis) δ^2H signals in streamflow based on varying the SAS shape parameter α [-] in the root zone for (a) HOAL and (b) Wüstebach. The simulations range from very young preference (α = 0.1) to old water preference (α = 5) for the unsaturated root zone preferential flow, while the groundwater flow was uniformly sampled (α = 1).

The Spearman rank correlations (r) between observed and simulated δ^2H were lower in HOAL compared to Wüstebach, which can be attributed in part to differences in temporal resolution and the variability of isotope sampling. In HOAL, streamflow δ^2H was sampled on an event basis, with values ranging from -26.2 ‰ to -108.0 ‰ (Fig. 1b). In contrast, the Wüstebach catchment weekly to biweekly sampling scheme yielded streamflow δ^2H values between -45.6 ‰ and -57.1 ‰ (Fig. 1b). For both catchments, root-zone preferential flow SAS functions from a preference for young water ($\alpha_0 = 0.1$) to old water ($\alpha_0 = 5.0$) influenced the TTD for ages up to 300 days ($T < 300$). This is consistent with root-zone storage residence times being predominantly shorter than 300 days (Fig. S 7a, c). Consequently, increasing α_0 from 0.1 to 5.0 and thus reducing the relative contribution of younger flows (Fig. 7a, b), shifted the empirical cumulative distribution functions (eCDFs) toward older water within the first 300 days. In the HOAL, the mean fraction of streamflow with $T < 300$ days reached about 10 % (Fig. 7a,) for all root-zone SAS formulations, whereas in Wüstebach, it was about 20 % (Fig. 7b). Overall, these results indicated that root-zone SAS functions with young-water preferences improved the fit to observed streamflow isotopes, highlighting the importance of preferential flow pathways in shaping short transit times and streams δ^2H interpretations.

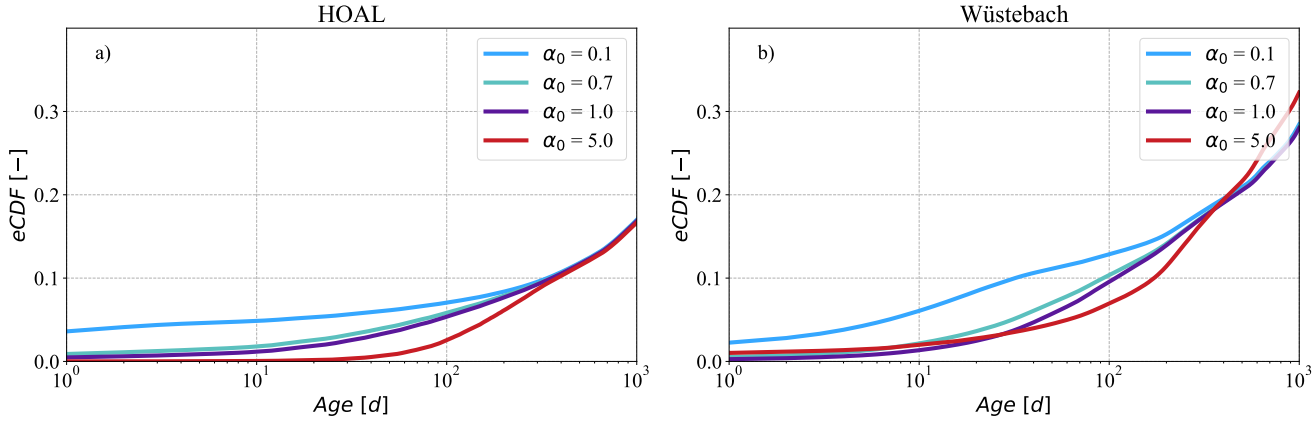

Figure 7. The mean of empirical cumulative distribution functions (eCDFs) of simulated transit times of daily discharge for the (a) HOAL and (b) Wüstebach catchments under varying SAS shape parameters in the unsaturated root zone ($\alpha_0 = 0.1, 0.7, 1.0, 5.0$). (a,b) The simulations range from very young preference (α_0 = 0.1) to old water preference (α_0 = 5) for the unsaturated root zone preferential flow, while the groundwater flow was uniformly sampled (α = 1).

Table 1. Performance metrics for δ^2H simulation results under various SAS parameter scenarios for the HOAL and Wüstebach catchments. The table includes the Nash- Sutcliffe efficiency ($NSE_{\delta^2\mathrm{H}}$) and mean absolute error ($MAE_{\delta^2\mathrm{H}}$), and Spearman rank correlation coefficients ($r_{\delta^2\mathrm{H}}$) based on SAS shape parameters (α_0) variations in the root zone and groundwater SAS shape parameters (α). Scenarios tested represent preferences for very young water ($\alpha = 0.1$), young water ($\alpha = 0.7$), uniform selection ($\alpha = 1.0$), and old water ($\alpha = 5.0$). For simulations testing SAS function variations in the root zone, the groundwater SAS function was kept uniform. Conversely, when testing groundwater SAS function variations, the root zone compartment was assigned its calibrated shape factor ($\alpha_0 = 0.14$ for HOAL and $\alpha_0 = 0.98$ for Wüstebach).

Catchment	**Metric**	**SAS Variation: Root Zone**				**SAS Variation: Groundwater**			
		$\alpha_0 = 0.1$	$\alpha_0 = 0.7$	$\alpha_0 = 1.0$	$\alpha_0 = 5.0$	$\alpha = 0.1$	$\alpha = 0.7$	$\alpha = 1.0$	$\alpha = 5.0$
HOAL	$\mathrm{NSE}_{\delta^2\mathrm{H}}$	0.56	0.28	0.15	-0.25	-0.83	0.55	0.56	0.55
	$\mathrm{MAE}_{\delta^2\mathrm{H}}$	2.46	2.85	3.06	4.02	4.75	2.54	2.48	2.48
	$\mathrm{r}_{\delta^2\mathrm{H}}$	0.55	0.35	0.24	-0.18	0.54	0.55	0.56	0.56
Wüstebach	$\mathrm{NSE}_{\delta^2\mathrm{H}}$	-0.14	0.47	0.51	-0.81	0.10	0.05	0.51	0.19
	$\mathrm{MAE}_{\delta^2\mathrm{H}}$	0.90	0.64	0.61	1.14	0.74	0.91	0.61	0.83
	$\mathrm{r}_{\delta^2\mathrm{H}}$	0.58	0.74	0.76	0.28	0.74	0.71	0.76	0.75

3.5 Sensitivity of δ^2H simulation and TTD estimation to different SAS functions for groundwater

The Spearman rank correlation coefficients (r) between simulated and observed δ^2H signals in streamflow, obtained by varying the SAS shape parameter α in groundwater, are shown in Figure 8. For the HOAL catchment, r values ranged from 0.54 to 0.60, indicating that, in contrast to the root-zone, changes in the groundwater SAS function had minimal impact on the fit

between simulated and observed δ^2H signals (Fig. 8a). In the Wüstebach catchment, r values only slightly increased from 0.71 ($\alpha = 0.1$) to 0.76 ($\alpha = 1.0$) before decreasing slightly at $\alpha = 5.0$ to 0.75. In both catchments, the correlations remained consistently strong across all α values tested (Fig. 8a, b).

A stronger preference for young water ($\alpha = 0.1$) led to approximately 25 % of streamflow being younger than 1000 days in the HOAL (Fig. 10a) and 35 % in the Wüstebach (Fig. 10b). In contrast, an older-water preference ($\alpha = 5.0$) shifted the distribution and reduced the proportion of streamflow being younger than 1000 days to 5% in the HOAL and to 12% in the Wüstebach. This shift, resulting from changing the SAS function parameter α from 0.1 to 5.0, produced a variability of approximately 20 % in HOAL and 23 % in Wüstebach in the proportion of streamflow composed of water younger than 1000 days (Fig. 10a, b).

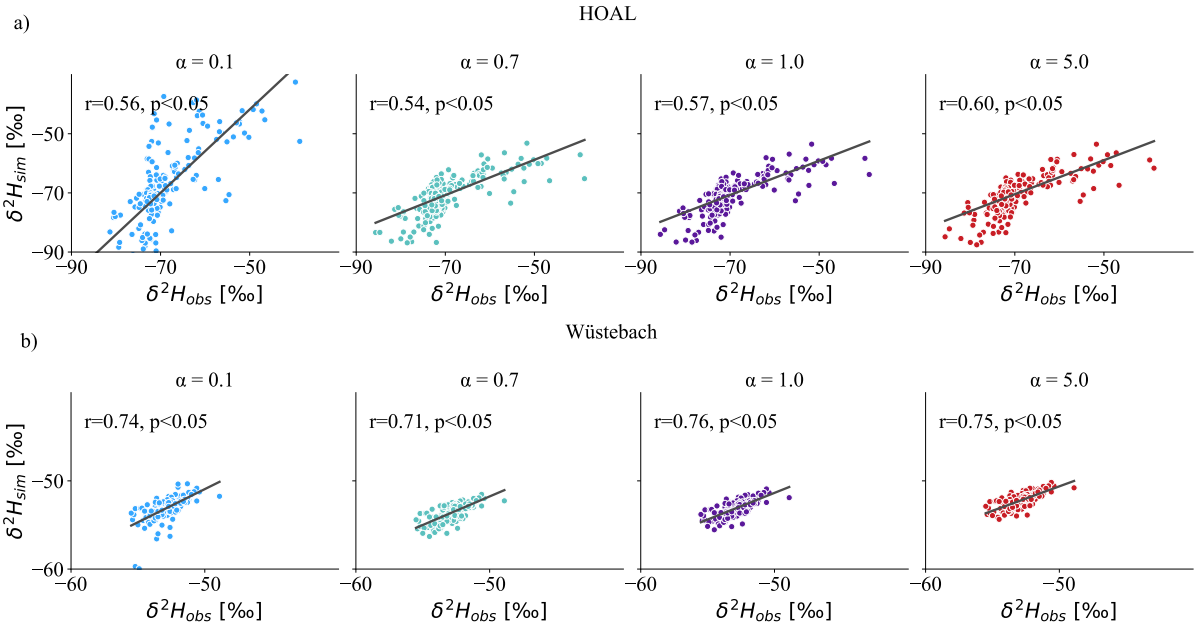

Figure 8. Spearman rank correlations between simulated (y-axis) and observed (x-axis) δ^2H signals in streamflow based on varying the SAS shape parameter α[-] in groundwater for (a) HOAL and (b) Wüstebach. The simulations ranged from very young water preference (α = 0.1) to old water preference (α = 5) for the groundwater, while for the root zone compartment, a calibrated value was used (α_0 = 0.14 for HOAL and 0.98 for Wüstebach).

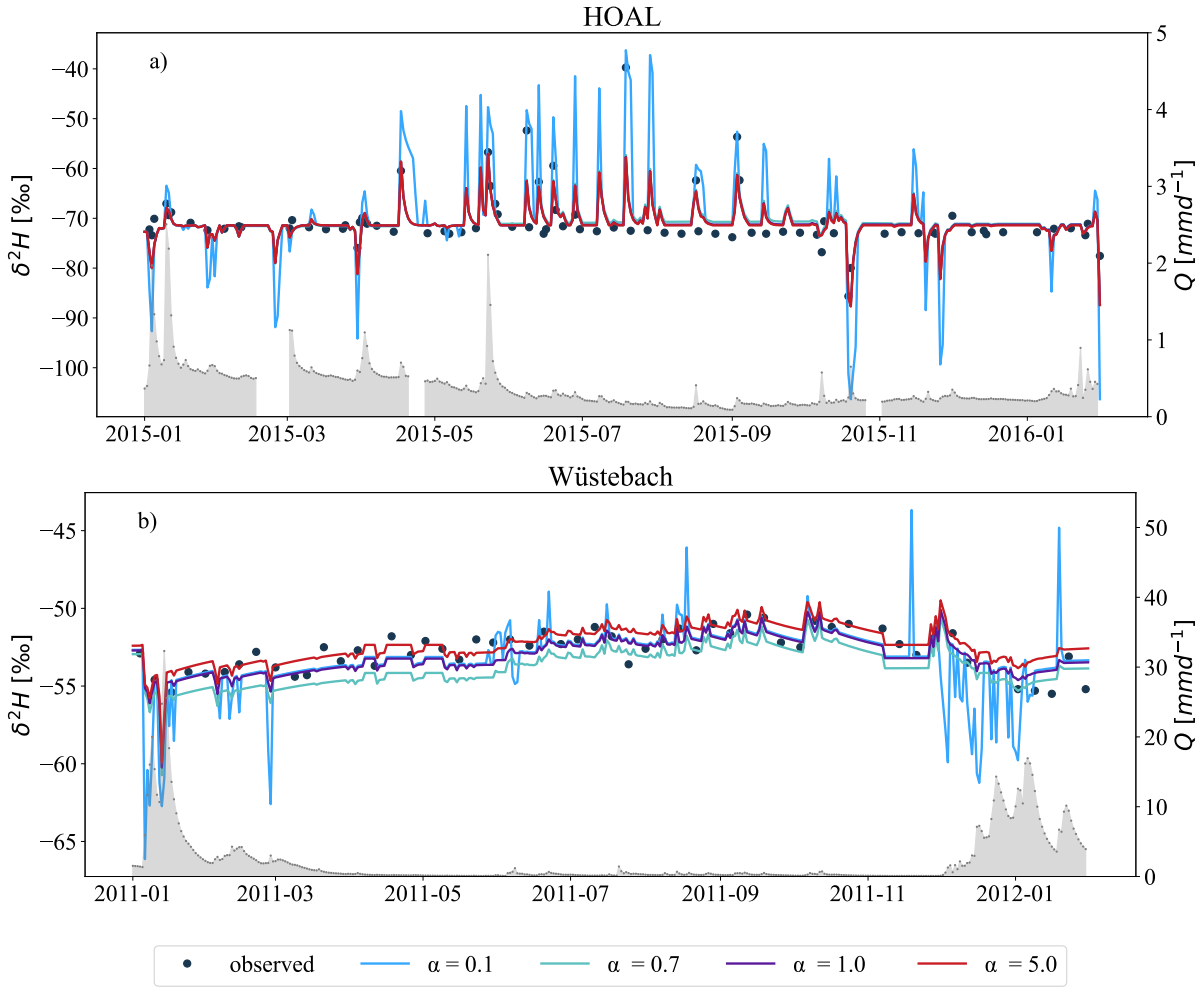

Figure 9. Simulation of δ^2H in streamflow based on varying SAS shape parameter α [-] in groundwater for (a) HOAL shown for 2015 and (b) Wüstebach shown for 2011. Simulations over the full tracking period are provided in Figure S 8. The simulations ranged from very young water preference (α = 0.1) to old water preference (α = 5) for the groundwater, while for the root zone compartment, a calibrated value was used (α_0 = 0.14, for HOAL and 0.98 for Wüstebach). The simulated $\delta^2 H$ signals from the model are illustrated with blue, turquoise, purple, and red lines corresponding to α values of 0.1, 0.7, 1.0, and 5.0, respectively. The grey-shaded area shows the measured streamflow (Q, mm d^{-1}) for both catchments.

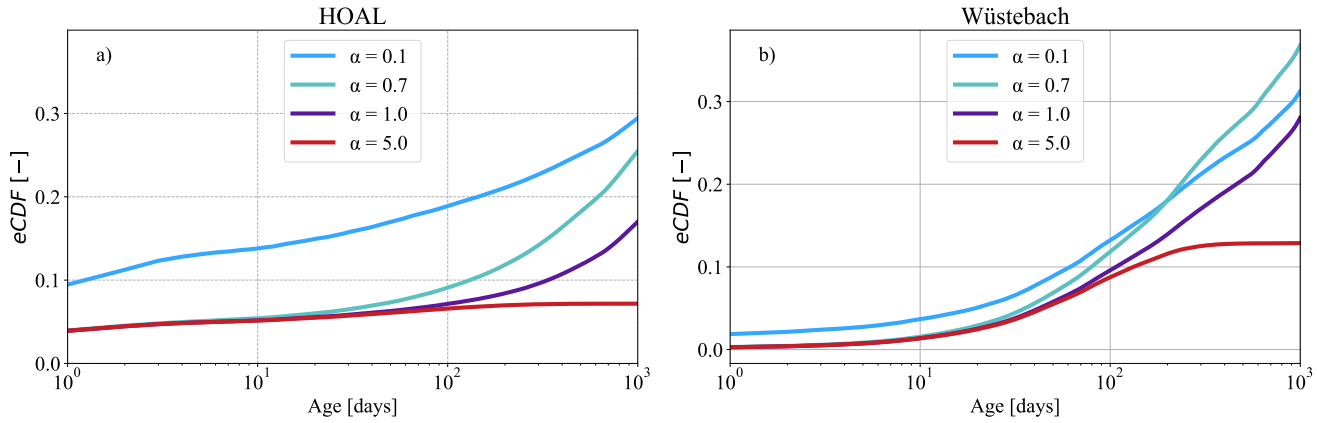

Figure 10. The mean of empirical cumulative distribution functions (eCDFs) of simulated transit times of daily discharge for the (a) HOAL and (b) Wüstebach catchments under varying SAS shape parameters ($\alpha = 0.1, 0.7, 1.0, 5.0$) for groundwater. Lower α values favour younger water, producing younger transit time distributions, while higher α values shift the distribution toward older water. The mean of inferred TTD lines are illustrated with blue, turquoise, purple, and red lines corresponding to α values of 0.1, 0.7, 1.0, and 5.0, respectively. The simulations ranged from very young water preference (α = 0.1) to old water preference (α = 5) for the groundwater, while for the root zone compartment, a calibrated value was used (α_0 = 0.14, for HOAL and 0.98 for Wüstebach).

3.6 Variation in the streamflow tracer signal and TTD estimations under different passive storage volumes and mixing assumptions

The results addressing the extent to which passive storage volume and associated mixing assumptions influence the representation of preferential groundwater flow, the estimated transit time distributions, and the interpretation of tracer signals at the catchment scale, are presented in Figures 11 and 12. Briefly, the findings show that increasing the passive storage volume dampens the contribution of young water, shifts the overall transit time distribution towards older ages, and reduces variability in the δ^2H signal variability in streamflow.

Simulations with varying $S_{S,p}$ volumes and different mixing assumptions (Figs. 11, 12) resulted in distinct δ^2H responses in streamflow. In both catchments, an active storage volume equivalent to approximately 1 % of the passive storage volume was needed to attenuate the simulated tracer signal in line with observations. In the HOAL, a passive storage volume of $S_{S,p} = 500$ mm (Fig. S 9a) was sufficient to achieve this, while in Wüstebach, a much larger volume of $S_{S,p} = 5000$ mm was necessary (Fig. S 9 b). SAS shape parameters indicating a young-water preference ($\alpha = 0.1$) resulted in variable δ^2H signals in streamflow, whereas an older-water preference ($\alpha = 5.0$) led to stronger dampening (Figs. 11, 12). Once the volume ratio between active and passive storage fell below 1 %, further increases in $S_{S,p}$ had little effect on model performance (Table 2). The NSE remained relatively stable across different $S_{S,p}$ values, with moderate improvements for $\alpha = 0.7$, 1.0, and 5.0. In contrast, simulations with $\alpha = 0.1$ yielded negative NSE values (Table 2). The highest $\text{NSE}_{\delta^2\text{H}}$ values—approximately 0.55—were achieved with $\alpha = 1.0$ and $\alpha = 5.0$ for the HOAL catchment. The results in the Wüstebach catchment exhibited a

wider range of NSE values, from –11.25 to 0.22, as $S_{S,p}$ increased, suggesting that model performance was more sensitive to the size of the passive storage volume than to the shape factor α.

In both catchments, increased passive storage volumes influenced the old tail of transit times ($100 < T < 1000$ days). Increasing $S_{S,p}$ increased the probability of older water contributing to streamflow (Figs. 11, 12) and reduced the fraction of streamflow younger than 1000 days substantially. The range of differences in the fraction of streamflow younger than 1000 days varied across different mixing assumptions, yet remained consistent overall. In the HOAL catchment (Fig. 11 a-c), under the uniform sampling assumption, the fraction of streamflow younger than 1000 days decreased from 50 % to 5 % as $S_{S,p}$ increased from 500 mm to 5000 mm. Given that model performance remained similar across these scenarios (Table 2), this implies a variability of approximately 45 % in TTD estimation attributable to uncertainties in passive storage volumes. In the Wüstebach catchment (Fig. 12 a-c), the corresponding fraction declined from 80 % to 45 %. None of the simulations with $S_{S,p}$ less than 5000 mm adequately reproduced the observed δ^2H signal, suggesting that at least 50 % of stream water in Wüstebach is older than 1000 days.

Table 2. Performance metrics for simulated δ^2H values in the HOAL (from 2015 to 2019) and Wüstebach (from 2011 to 2013) catchments under varying passive groundwater storage volumes ($S_{s,p}$) and groundwater SAS function shape parameters (α). For each $S_{s,p}$ volume (500 mm, 1000 mm, and 5000 mm), simulations were run with α values representing a range from very young-water preference (α = 0.1) to old-water preference (α = 5.0). The root zone SAS function was fixed at its calibrated value for each catchment (α_0 = 0.14 for HOAL and 0.98 for Wüstebach). Performance was evaluated using the Nash–Sutcliffe Efficiency (NSE_{δ^2H}) and Mean Absolute Error (MAE_{δ^2H}) between observed and simulated streamflow δ^2H signals.

Catchment	**Metric**	$S_{s,p} = 500\,mm$				$S_{s,p} = 1000\,mm$				$S_{s,p} = 5000\,mm$			
	$\alpha =$	0.1	0.7	1.0	5.0	0.1	0.7	1.0	5.0	0.1	0.7	1.0	5.0
	NSE_{δ^2H}	-1.20	0.49	0.55	0.55	-1.02	0.53	0.55	0.56	-0.68	0.55	0.56	0.56
HOAL	MAE_{δ^2H}	5.34	2.92	2.60	2.67	5.00	2.70	2.51	2.50	4.55	2.53	2.49	2.49
	NSE_{δ^2H}	-11.25	-12.52	-13.34	-12.17	-5.77	-7.58	-6.88	-8.08	0.14	-0.44	0.31	0.22
Wüstebach	MAE_{δ^2H}	3.70	3.74	4.04	3.64	2.77	3.05	3.04	2.84	0.77	1.16	0.76	0.81

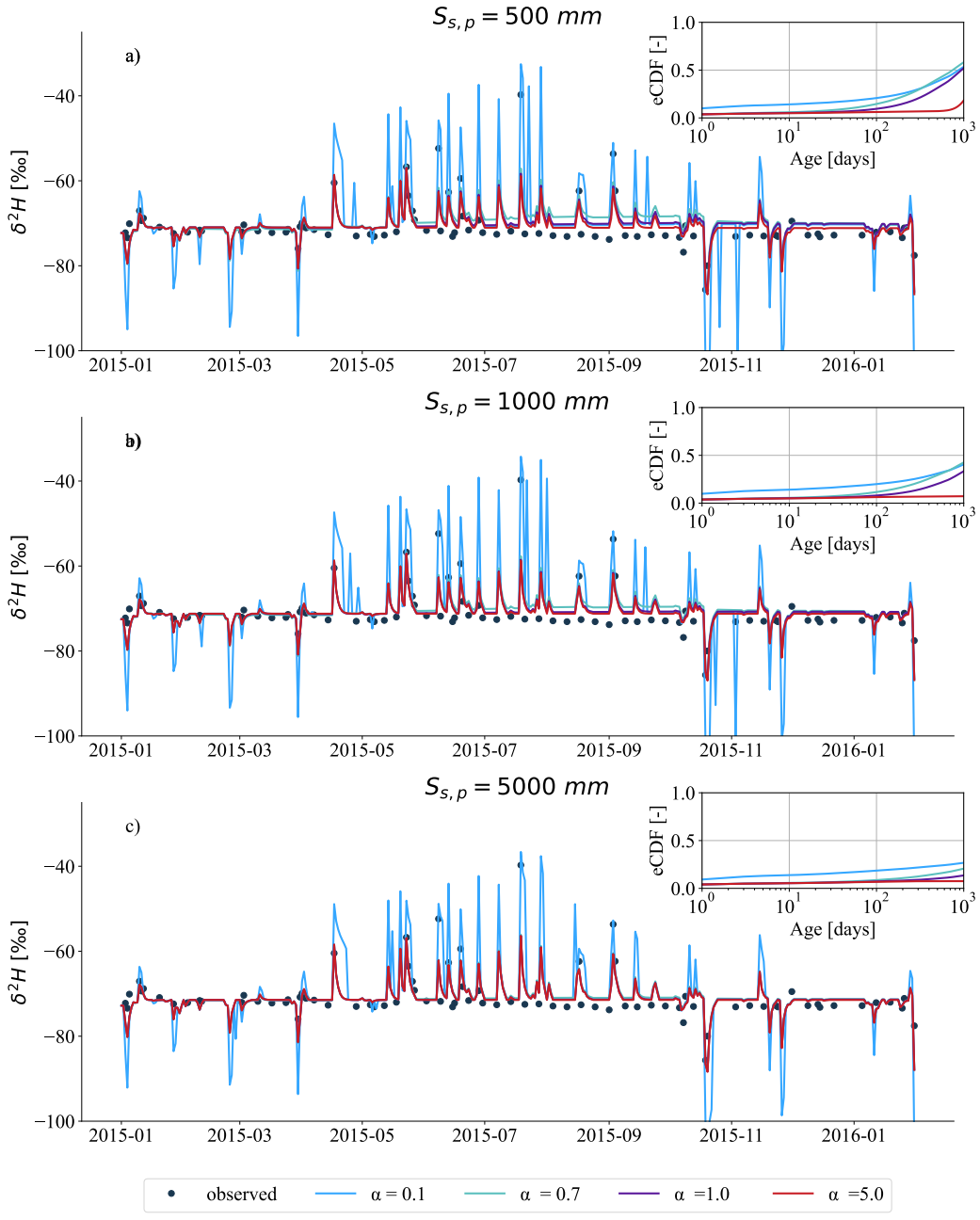

Figure 11. Simulated δ^2H signals in streamflow (Q; mm d^{-1}) for the HOAL catchment in the year 2015, based on varying passive groundwater storage volumes ($S_{S,p}$ = 500 mm, 1000 mm, and 5000 mm) and different mixing assumptions defined by SAS function shape parameters (α = 0.1, 0.7, 1.0, and 5.0). (a-c) each plot shows results for one $S_{S,p}$ value, with black dots indicating observed grab samples of streamflow δ^2H, and coloured lines representing simulated δ^2H under the different α values. The inset in each plot shows the mean empirical cumulative distribution functions (CDF) of simulated daily streamflow transit times during the tracking period (2015–2019); line colours correspond to α values: blue for 0.1, turquoise for 0.7, purple for 1.0, and red for 5.0. Simulations over the full tracking period (2015–2019) are provided in the Supplement S 10.

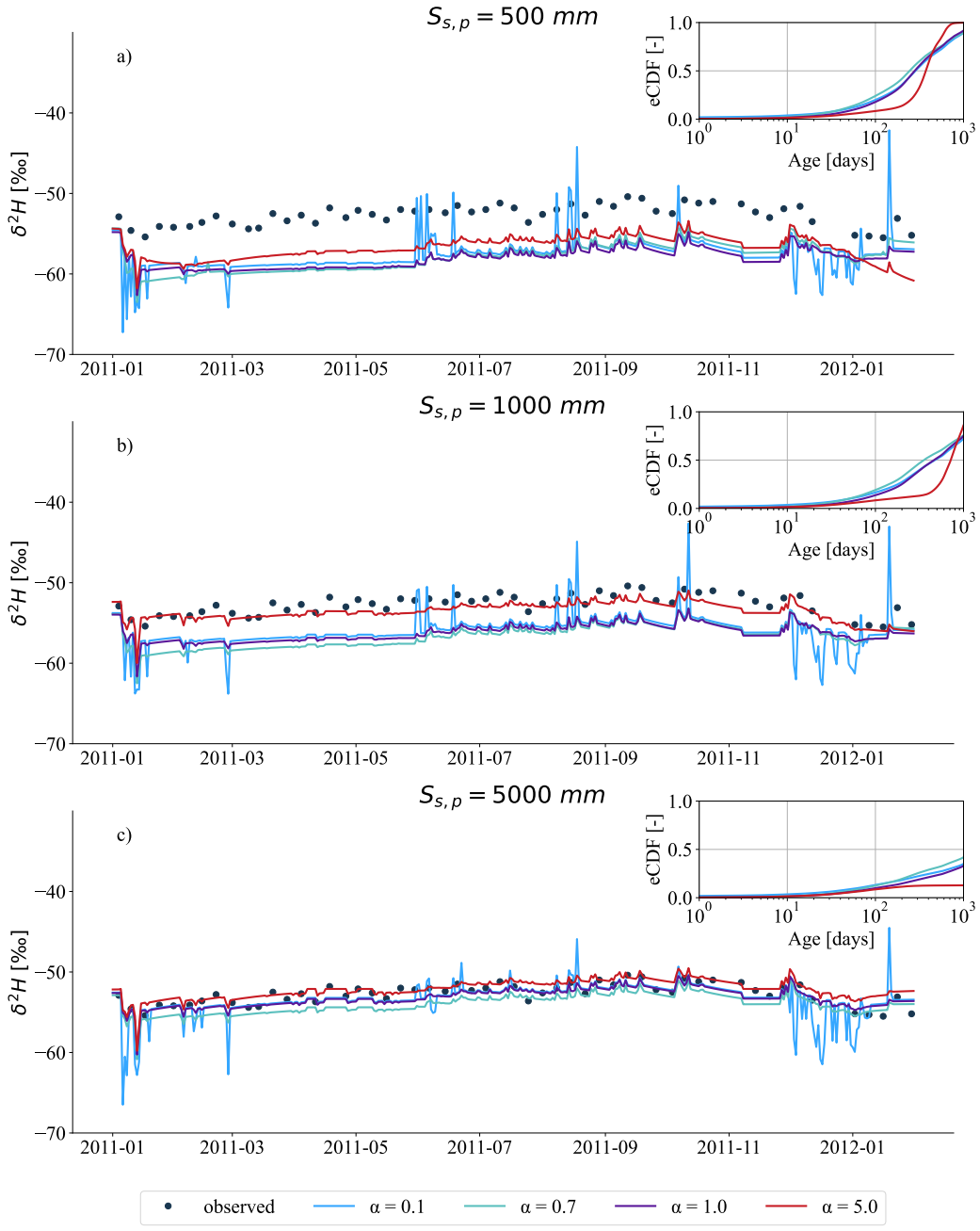

Figure 12. Simulated δ^2H signals in streamflow (Q; mm d^{-1}) for the Wüstebach catchment in the year 2011, based on varying passive groundwater storage volumes ($S_{S,p}$ = 500 mm, 1000 mm, and 5000 mm) and different mixing assumptions defined by SAS function shape parameters (α = 0.1, 0.7, 1.0, and 5.0). (a-c) each plot shows results for one $S_{S,p}$ value, with black dots indicating observed grab samples of streamflow δ^2H, and coloured lines representing simulated δ^2H under the different α values. The inset in each plot shows the mean empirical cumulative distribution functions (eCDFs) of simulated daily streamflow transit times during the tracking period. Line colours correspond to α values: blue for 0.1, turquoise for 0.7, purple for 1.0, and red for 5.0. Simulations over the full tracking period (2011–2013) are provided in the Supplement S 11.

4 Discussion

4.1 Comparison of catchment transit times

The inferred transit times in HOAL (13 % of streamwater younger than 1000 days) and Wüstebach (27 % of streamwater younger than 1000 days) indicated that, in both catchments, the majority of water contributing to streamflow was relatively old—consistent with findings from many other catchments (Kirchner et al., 2023; Floriancic et al., 2024; Wang et al., 2025). During wet periods, the fraction of water $T < 1000$ days was 15 % in HOAL and 33 % in Wüstebach; in dry periods, these values dropped to 10 % and 22 %, respectively. This variation indicated a greater release of younger water under wetter conditions, consistent with other studies (Klaus et al., 2013; Angermann et al., 2017; Loritz et al., 2017). In Wüstebach, relatively high soil wetness and high monthly mean young-water fractions ranging from 5 % to 15 % (Figs. 5e, f) pointed to wet-soil promotion of preferential flow which has been observed previously (Wiekenkamp et al., 2016; Stockinger et al., 2014; Hrachowitz et al., 2021; Hövel et al., 2024). By contrast, HOAL's younger-water release did not depend on soil wetness only; instead, rapid flow pathways (e.g. infiltration-excess overland flow, macropores, tile drains) as known for this catchment (Exner-Kittridge et al., 2016; Pavlin et al., 2021; Vreugdenhil et al., 2022) allowed water to bypass much of the soil matrix and reach the stream quickly, even under dry conditions, which was discussed in previous findings (Türk et al., 2024; Széles et al., 2020). The consistency of our results with prior tracer-based modeling and SAS applications in both HOAL (Széles et al., 2020; Türk et al., 2024) and Wüstebach (Stockinger et al., 2019; Hrachowitz et al., 2021) provides confidence in the applied model configurations. However, we acknowledge that such consistency alone cannot exclude the possibility of shared assumptions. Therefore, we use these results as supporting evidence that the model setups are reasonable for testing the research hypotheses, while recognizing the need for further validation with complementary data and approaches.

4.2 Do stream water tracer data have sufficient variability to identify preferential flow in the unsaturated root zone and in groundwater using different SAS functions?

Positive correlations between modeled and observed streamflow tracer signals (Fig. 6a,b), together with high model-efficiency metrics at lower α_0 values (indicating a preference for younger water; Table 1), show that streamflow tracer data were sufficiently sensitive to the SAS parameterization of preferential flow in the unsaturated zone for both the HOAL and Wüstebach catchments. This suggests rapid transport of precipitation through preferential flow pathways in both catchments, consistent with previous findings (Wiekenkamp et al., 2016; Stockinger et al., 2014; Széles et al., 2020). Specifically, changing the root-zone SAS shape parameter α_0 produced clear differences in simulated streamflow δ^2H signals (Fig. 6), demonstrating tracer-data sensitivity to young-water release. The results, quantitatively demonstrated through the SAS-based modeling framework, show that streamflow isotope data can reflect the activation of preferential flow in the unsaturated zone. While previous studies have identified such processes through field observations (Vreugdenhil et al., 2022; Pavlin et al., 2021; Wiekenkamp et al., 2016), our results demonstrate that they can also be captured and interpreted using catchment-scale tracer modeling.

Nevertheless, the two catchments exhibited distinct processes controlling preferential flow in the unsaturated root zone. The calibrated lower boundary of the SAS function shape parameter, α_0, differed markedly ($\alpha_0 = 0.14$ for HOAL and $\alpha_0 = 0.98$

for Wüstebach), reflecting contrasting storage–discharge relationships and preferential flow activation mechanisms in the unsaturated zone. In HOAL, the low α_0 value indicated rapid, direct water transmission through preferential flow paths driven by intense rainfall, consistent with previous hydrometric analyses and field observations (Pavlin et al., 2021; Vreugdenhil et al., 2022), which allow young water to reach the stream with limited mixing. This was further facilitated by the formation of soil crusts and cracking of the clay-rich topsoil during the dry summer months, creating direct preferential pathways that accelerate water transmission through the catchment (Exner-Kittridge et al., 2016). In contrast, the higher α_0 value in Wüstebach ($\alpha_0 = 0.98$) indicated that under wetter antecedent conditions, established preferential flow pathways promoted greater subsurface mixing, leading to relatively older water contributions. This likely reflects the influence of forest cover in Wüstebach, where enhanced infiltration promotes deeper and more uniform mixing (Wiekenkamp et al., 2016) than in HOAL. Despite contrasting site characteristics, both catchments showed responses consistent with previous studies that documented the role of macropores and preferential flow pathways in the unsaturated zone, where water frequently bypasses matrix storage and exchange processes (Zehe et al., 2006; Angermann et al., 2017; Sprenger et al., 2016; Klaus et al., 2013; Loritz et al., 2017).

On the other hand, streamflow tracer δ^2H showed limited sensitivity to variations in groundwater SAS function shape parameters (Fig. 8, Table 1), suggesting that isotope data alone may not provide sufficient variability to resolve preferential groundwater flow dynamics at the catchment scale. This is supported by the small variation in correlation strength across different α settings, with $r = 0.54$–0.60 in the HOAL catchment and $r = 0.71$–0.76 in Wüstebach. We attributed this limited variability to the large passive groundwater storage volumes formulated within the model (approximately 500 mm in HOAL and 5000 mm in W"ustebach;), which act to buffer hydrological variability and result in comparable model performance once the storage threshold is exceeded Table 2). It should be noted that these values represent modeled estimates rather than their actual physical magnitude and therefore reflect a parameterization that buffers the effect of preferential groundwater flow on δ^2H simulations. In our and many other catchment scale modelling approaches (Benettin et al., 2015a; Hrachowitz et al., 2013; Wang et al., 2023, 2025), groundwater (Q_S) age selection is formulated based on age samples from the total groundwater storage ($S_{S,\text{tot}}$), combining contributions from both active ($S_{S,a}$) and passive ($S_{S,p}$) compartments (Zuber, 1986; Hrachowitz et al., 2015). Thus, the age-ranked groundwater storage ($S_{T,S,\text{tot}}$) inherently reflected a mixture of these storage volumes. Although the model explicitly allowed preferential recharge of younger groundwater (e.g, R_{fs}, Fig. 2), the passive storage, characterized by long residence times, buffers the isotopic signals in streamflow (Birkel et al., 2011a), thereby masking the distinct signatures of preferential groundwater flow. Consequently, varying the groundwater SAS shape had limited effects on simulated streamflow δ^2H dynamics within the parameter ranges tested here.

The Spearman rank correlations (r) between observed and simulated δ^2H were lower in HOAL compared to Wüstebach, which can be attributed to differences in temporal resolution and the variability of isotope sampling (Fig. 1a, b). Although model performance metrics, such as NSE or correlation coefficients, quantify the agreement between simulated and observed isotope time series, they can result in seemingly good fits in the presence of sparse or irregular data sampling (Beven, 2006). In such cases, deceptively high NSE values may still occur even when key groundwater age-selection parameters (e.g., preference for young vs. old water) remain poorly constrained, thereby affecting transit time estimations (Stockinger et al., 2016).

4.3 Does accounting for preferential flow through a SAS function affect catchment-scale transit time distributions?

Different groundwater mixing assumptions yielded similar isotope model fits (Table 2), except for the case with a strong young-water preference ($\alpha = 0.1$) in the HOAL catchment. However, the corresponding transit time distributions (TTDs) differed substantially, revealing that TTD estimates remain highly uncertain with the available isotope data. Consistent with previous studies (van der Velde et al., 2012; Borriero et al., 2023), our findings emphasize that TTDs are particularly sensitive to how groundwater SAS functions are conceptualized and parameterized within the model.

Specifically, assuming a strong young-water preference ($\alpha = 0.1$) yielded fractions of streamflow younger than 1000 days of approximately 25 % in HOAL and 35 % in Wüstebach, whereas an older-water preference ($\alpha = 5.0$) reduced these fractions to around 5 % and 12 %, respectively (Fig. 10). This variability in transit time estimates for $T < 1000$ days—about 20 % in HOAL and 23 % in Wüstebach—highlights a key limitation: groundwater transit times derived from SAS functions remain highly uncertain, even when overall model performance is similar.

4.4 How do groundwater mixing assumptions and passive storage volumes influence tracer simulation and transit time estimation at the catchment scale?

In both HOAL and Wüstebach catchments, isotope signals were attenuated when the ratio between active and passive storage ($S_{S,a}/S_{S,p}$) fell below 1 % (Figs. 11, 12). This indicates that the passive groundwater storage was much larger—typically about one order of magnitude greater than the active storage, as also reported by Birkel et al. (2011a)—and acted as an effective buffer that dampened isotope variability in streamflow and constrained the model's ability to resolve young-water dynamics.

In HOAL, model performance remained comparable across a wide range of passive storage volumes above 500 mm (e.g., $\mathrm{NSE}_{\delta^2 H} \approx 0.55$), suggesting considerable uncertainty in the upper bound of passive storage for any volume exceeding this threshold. In contrast, model performance in Wüstebach improved with increasing passive storage (Table 2), consistent with previous findings by Hrachowitz et al. (2021), who proposed substantial groundwater storage (∼8000 mm) to reproduce observed isotope damping. Nevertheless, the stepwise analysis showed that similar performance ($\mathrm{NSE}_{\delta^2 H} = 0.31$) could also be achieved with $S_{S,p} = 5000$ mm and uniform mixing, reinforcing the large uncertainty in constraining the upper range of passive storage volumes in catchment-scale models. Given the uncertainties in passive storage parameters, it is crucial to assess how passive groundwater storage, combined with active storage, influences estimated transit time distributions (TTDs). In both catchments, a clear negative correlation emerged between passive storage volume and the fraction of streamflow younger than 1000 days (Figs. 11, 12). Under uniform sampling assumptions, the young-water fraction decreased from approximately 45 % to 10 % in HOAL and from about 85 % to 25 % in Wüstebach as $S_{S,p}$ increased from 500 mm to 5000 mm. The SAS function was formulated based on total groundwater storage ($S_{S,\mathrm{tot}} = S_{S,a} + S_{S,p}$), larger passive storage volumes increased the likelihood of older water contributions to streamflow, thereby extending the tails of the TTDs ($100 < T < 1000$ days).

4.5 Implications and limitations

The methodological framework applied here, including the stepwise analysis of SAS functions and the incorporation of multiple passive storage volumes, offered a systematic approach that could be adapted to other regions and TTD studies. Nonetheless, the uncertainty resulting from the specific model setup and parameter choices used in this study cannot be directly generalised across diverse catchments or hydrological conditions. Addressing these limitations, for example, by improving the monitoring frequency of (isotope) hydrological data, integrating additional tracers such as tritium (^3H), and refining model representations of subsurface processes, will be essential for reducing uncertainty and enhancing the reliability of SAS-based modeling.

While our study focused on a lumped catchment-scale framework, the results highlighted the need to advance toward more distributed models that can more directly link spatial heterogeneity in soils, slopes, and storage to preferential flow dynamics and advance process understanding. At the catchment scale, isotope-based modeling proved useful in capturing preferential flow in the unsaturated zone, but was limited in doing so in groundwater due to the damping of the seasonal signal of water stable isotopes by large passive storage volumes assumed in the models. This suggests that in catchments with similar damped water stable isotope signals, groundwater age selection will be difficult to constrain.

While the SAS formulation identifies the statistical signatures of preferential flow through tracer-based modeling, it does not explicitly resolve the physical mechanisms that induce preferential flow. Therefore, isotope data alone, when used within a catchment-scale lumped model framework, may be insufficient to distinguish between a true absence of preferential flow and a limited model sensitivity to detect it. In the HOAL catchment, Exner-Kittridge et al. (2016) showed that alternating contributions from shallow and deep aquifers throughout the year were the main cause of the seasonal variability in nitrate concentrations in streamflow. These alternating contributions, together with extensive tile drainage and heterogeneous clay-rich soils, create rapid and spatially variable flow pathways (Exner-Kittridge et al., 2016; Pavlin et al., 2021). Such features, combined with overland flow of the HOAL catchment (Blöschl et al., 2016), may favor the activation of preferential flow. For the Wüstebach catchment, field studies indicated that soil and groundwater dynamics are coupled. Bogena et al. (2015) and Graf et al. (2014) showed that soil water variability decreases with depth due to lower porosity and root water uptake in shallow depth, while groundwater fluctuations closely follow soil moisture dynamics (Bogena et al., 2015), reflecting high infiltration and storage capacity in forest soils. This behaviour contrasts with the results obtained in the HOAL catchment, suggesting a more uniform subsurface mixing in Wüstebach. Although these processes remain beyond the explicit resolution of top-down, isotope-based transport models, the SAS framework enables delineation of the hydrological conditions under which preferential flow effects become detectable. Future research should combine stable isotopes with complementary tracers (e.g., tritium, chloride, or major ions) and higher-frequency sampling to enhance the diagnostic power of tracer-aided models. Furthermore, linking SAS function shapes to measurable catchment attributes could enable *a priori* parameterization, thereby reducing dependence on calibration. At the lysimeter pedon scale, Asadollahi et al. (2020) showed that SAS functions can approximate the analytical solution of the advection–dispersion equation; however, extending such mechanistic relationships to the catchment scale remains challenging within lumped "bucket" model frameworks. Addressing these challenges represents

a key step toward integrating empirical SAS modeling with a process-based understanding of preferential flow and subsurface mixing.

5 Conclusion

In this study, we evaluated whether stream water isotope data contain sufficient variability to simulate preferential flow in the unsaturated zone and in groundwater using various StorAge Selection (SAS) function parametrizations within a catchment-scale transport model. We further analysed the implications of explicitly representing preferential root-zone and groundwater flow, as well as passive storage volumes, on the estimation of transit time distributions (TTDs). The findings indicated that streamflow tracer data were sufficiently sensitive to the SAS parameterization of preferential flow in the shallow unsaturated zone. However, the results also revealed critical limitations in using isotope tracer data alone to constrain groundwater transit times, due to the strong influence of passive groundwater storage on model uncertainty at the catchment scale.

The main findings of our study are:

- Streamflow isotope (δ^2H) data were sensitive enough to characterise preferential flow processes in the unsaturated root zone, confirming that such processes significantly shape catchment isotope signatures and transit time distributions at short timescales (up to 300 days).
- Streamflow isotope data alone were insufficient to differentiate among groundwater SAS function shapes for the two tested catchments. Large passive groundwater storage volumes significantly dampened isotopic variations, making it impossible to clearly identify preferential flow in groundwater.
- The variability in groundwater TTD estimates arising from varying SAS function shapes for groundwater was considerable (20 % for HOAL and 23 % for Wustebach), highlighting that TTD estimates are highly sensitive to how SAS functions are conceptualised and parameterised within the model.
- The size of the passive groundwater storage exerts a dominant control on catchment transit time estimates, particularly influencing the longer tails ($T > 100$ days) of the distributions, thereby introducing uncertainties into solute and contaminant transport predictions.

These findings carry implications beyond water transit times, also affecting the transport timescales of solutes and contaminants within catchments. Larger passive storage volumes imply prolonged retention times, potentially delaying pollutant transport and release. Consequently, uncertainty in estimating passive storage volumes directly translates into uncertainty regarding contaminant transport predictions, with critical implications for assessing water-quality risks. Additional or complementary datasets—such as direct groundwater measurements or higher-frequency tracer sampling—would be required to reliably characterise preferential groundwater flow using conceptual catchment-scale models. Improved characterisation of passive storage volumes—potentially via complementary observations (e.g., groundwater-level monitoring or high-frequency

isotope sampling)—is essential to reduce uncertainties and enhance reliability in transit time and solute transport modelling at the catchment scale.

Code and data availability. A Python script that performs the calculations described in this paper will be deposited in an open-access Github archive repository, and the link will be supplied with the final published paper. The code repository for the *Tracer Transport Model* is available on GitHub at: https://github.com/haticeturk/Tracer_Transport_Model.git. Model outputs, including state variables, fluxes, hydrological signatures, parameter sets, and performance metrics underlying this study, are available online in the FAIR-compliant Zenodo repository. The meteorological and hydrological data from the Wüstebach TERENO site used in this study are openly accessible through the *Terrestrial Environmental Observatories (TERENO)* of the *Helmholtz Association of German Research Centers (HGF), Germany*, via the TEODOOR data portal (http://teodoor.icg.kfa-juelich.de/). The stable water isotope dataset for the Wüstebach catchment is publicly available through a digital object identifier (DOI) at: https://doi.org/10.34731/y6tj-3t38 (Bogena et al., 2021). The data for the HOAL catchment can be available from the Austrian Federal Agency for Water Management upon request.

Author contributions. HT performed the analysis presented here and drafted the paper. All authors discussed the design, contributed to the overall concept, and participated in the discussion and writing of the manuscript.

Competing interests. Some authors are members of the editorial board of the HESS journal.

Acknowledgements. We acknowledge the *Terrestrial Environmental Observatories (TERENO)* of the *Helmholtz Association of German Research Center (HGF), Germany*, for providing access to the Wüstebach catchment data. We thank the Austrian Federal Agency for Water Management for providing the data the HOAL catchment that we used in our analysis. This research was funded by the *Austrian Science fully Fund by (FWF – Österreichischer Wissenschaftsfonds)* [Grant No. 10.55776/P34666]. For open access purposes, the author has applied a CC BY public copyright license to any author-accepted manuscript version arising from this submission. The work of Hatice Türk was supported by the Doctoral School "Human River Systems in the 21st Century (HR21)" of the BOKU University, Vienna.

References

Ala-Aho, P., Tetzlaff, D., McNamara, J. P., Laudon, H., and Soulsby, C.: Using isotopes to constrain water flux and age estimates in snow-influenced catchments using the STARR (Spatially distributed Tracer-Aided Rainfall–Runoff) model, Hydrology and Earth System Sciences, 21, 5089–5110, 2017.

Angermann, L., Jackisch, C., Allroggen, N., Sprenger, M., Zehe, E., Tronicke, J., Weiler, M., and Blume, T.: Form and function in hillslope hydrology: characterization of subsurface flow based on response observations, Hydrology and Earth System Sciences, 21, 3727–3748, 2017.

Asadollahi, M., Stumpp, C., Rinaldo, A., and Benettin, P.: Transport and water age dynamics in soils: A comparative study of spatially integrated and spatially explicit models, Water Resources Research, 56, no–no, 2020.

Benettin, P. and Bertuzzo, E.: tran-SAS v1.0: a numerical model to compute catchment-scale hydrologic transport using StorAge Selection functions, Geoscientific Model Development, 11, 1627–1639, 2018.

Benettin, P., Kirchner, J., Rinaldo, A., and Botter, G.: Modeling chloride transport using travel time distributions at Plynlimon, Wales, Water Resources Research, 51, 3259–3276, https://doi.org/10.1002/2014WR016600, 2015a.

Benettin, P., Rinaldo, A., and Botter, G.: Tracking residence times in hydrological systems: Forward and backward formulations, Hydrological Processes, 29, 5203–5213, https://doi.org/10.1002/hyp.10513, 2015b.

Berkowitz, B. and Zehe, E.: Surface water and groundwater: unifying conceptualization and quantification of the two "water worlds", Hydrology and Earth System Sciences, 24, 1831–1858, https://doi.org/10.5194/hess-24-1831-2020, 2020.

Berkowitz, B., Cortis, A., Dentz, M., and Scher, H.: Modeling non-Fickian transport in geological formations as a continuous time random walk, Reviews of Geophysics, 44, 2006.

Beven, K.: A manifesto for the equifinality thesis, Journal of Hydrology, 320, 18–36, https://doi.org/10.1016/j.jhydrol.2005.07.007, 2006.

Beven, K. and Germann, P.: Macropores and water flow in soils, Water resources research, 18, 1311–1325, 1982.

Bianchi, M., Zheng, C., Wilson, C., Tick, G. R., Liu, G., and Gorelick, S. M.: Spatial connectivity in a highly heterogeneous aquifer: From cores to preferential flow paths, Water Resources Research, 47, 2011.

Birkel, C., Soulsby, C., and Tetzlaff, D.: Modelling catchment-scale water storage dynamics: Reconciling dynamic storage with tracer inferred passive storage, Hydrological Processes, 25, 3924–3936, https://doi.org/10.1002/hyp.8201, 2011a.

Birkel, C., Tetzlaff, D., Dunn, S. M., and Soulsby, C.: Using lumped conceptual rainfall–runoff models to simulate daily isotope variability with fractionation in a nested mesoscale catchment, Advances in Water Resources, 34, 383–394, 2011b.

Birkel, C., Soulsby, C., and Tetzlaff, D.: Conceptual modelling to assess how the interplay of hydrological connectivity, catchment storage and tracer dynamics controls nonstationary water age estimates, Hydrological Processes, 29, 2956–2969, 2015.

Blöschl, G., Blaschke, A. P., Broer, M., Bucher, C., Carr, G., Chen, X., Eder, A., Exner-Kittridge, M., Farnleitner, A., Flores-Orozco, A., Haas, P., Hogan, P., Kazemi Amiri, A., Oismüller, M., Parajka, J., Silasari, R., Stadler, P., Strauss, P., Vreugdenhil, M., and Zessner, M.: The Hydrological Open Air Laboratory (HOAL) in Petzenkirchen: a hypothesis-driven observatory, Hydrology and Earth System Sciences, 20, 227–255, https://doi.org/10.5194/hess-20-227-2016, 2016.

Bogena, H. R., Bol, R., Borchard, N., Brüggemann, N., Diekkrüger, B., Drüe, C., Groh, J., Gottselig, N., Huisman, J. A., Lücke, A., et al.: A terrestrial observatory approach to the integrated investigation of the effects of deforestation on water, energy, and matter fluxes, Science China Earth Sciences, 58, 61–75, 2015.

Bogena, H. R., Montzka, C., Huisman, J. A., Graf, A., Schmidt, M., Stockinger, M., von Hebel, C., Hendricks-Franssen, H. J., van der Kruk, J., Tappe, W., Lücke, A., Baatz, R., Bol, R., Groh, J., Pütz, T., Jakobi, J., Kunkel, R., Sorg, J., and Vereecken, H.: The TERENORur Hydrological Observatory: A Multiscale MultiCompartment Research Platform for the Advancement of Hydrological Science, Vadose Zone Journal, 17, 1–22, https://doi.org/10.2136/vzj2018.03.0055, 2018.

Bogena, H. R., Stockinger, M. P., and Lücke, A.: Long-term stable water isotope and runoff data for the investigation of deforestation effects on the hydrological system of the Wüstebach catchment, Germany, Hydrological processes, 35, e14 006, 2021.

Borriero, A., Kumar, R., Nguyen, T. V., Fleckenstein, J. H., and Lutz, S. R.: Uncertainty in water transit time estimation with StorAge Selection functions and tracer data interpolation, Hydrology and Earth System Sciences, 27, 2989–3004, https://doi.org/10.5194/hess-27-2989-2023, 2023.

Botter, G., Bertuzzo, E., and Rinaldo, A.: Catchment residence and travel time distributions: The master equation, Geophysical Research Letters, 38, 1–6, https://doi.org/10.1029/2011GL047666, 2011.

Exner-Kittridge, M., Strauss, P., Blöschl, G., Eder, A., Saracevic, E., and Zessner, M.: The seasonal dynamics of the stream sources and input flow paths of water and nitrogen of an Austrian headwater agricultural catchment, Science of the Total Environment, 542, 935–945, https://doi.org/10.1016/j.scitotenv.2015.10.151, 2016.

Fenicia, F., Savenije, H. H., Matgen, P., and Pfister, L.: Is the groundwater reservoir linear? Learning from data in hydrological modelling, Hydrology and Earth System Sciences, 10, 139–150, https://doi.org/10.5194/hess-10-139-2006, 2006.

Fenicia, F., Wrede, S., Kavetski, D., Pfister, L., Hoffmann, L., Savenije, H. H., and McDonnell, J. J.: Assessing the impact of mixing assumptions on the estimation of streamwater mean residence time, Hydrological Processes, 24, 1730–1741, 2010.

Floriancic, M. G., Stockinger, M. P., Kirchner, J. W., and Stumpp, C.: Monthly new water fractions and their relationships with climate and catchment properties across Alpine rivers, Hydrology and Earth System Sciences, 28, 3675–3694, 2024.

Fovet, O., Ruiz, L., Hrachowitz, M., Faucheux, M., and Gascuel-Odoux, C.: Hydrological hysteresis and its value for assessing process consistency in catchment conceptual models, Hydrology and Earth System Sciences, 19, 105–123, 2015.

Graf, A., Bogena, H. R., Drüe, C., Hardelauf, H., Pütz, T., Heinemann, G., and Vereecken, H.: Spatiotemporal relations between water budget components and soil water content in a forested tributary catchment, Water Resources Research, 50, 4837–4857, https://doi.org/10.1002/2013wr014516, 2014.

Hamilton, S. K.: Biogeochemical time lags may delay responses of streams to ecological restoration, Freshwater Biology, 57, 43–57, 2012.

Hansen, S. K. and Berkowitz, B.: Aurora: A non-Fickian (and Fickian) particle tracking package for modeling groundwater contaminant transport with MODFLOW, Environmental Modelling & Software, 134, 104 871, 2020a.

Hansen, S. K. and Berkowitz, B.: Modeling non-Fickian solute transport due to mass transfer and physical heterogeneity on arbitrary groundwater velocity fields, Water Resources Research, 56, e2019WR026 868, 2020b.

Harman, C.: Age-ranked storage-discharge relations: A unified description of spatially lumped flow and water age in hydrologic systems, Water Resources Research, 55, 7143–7165, 2019.

Harman, C. J.: Time-variable transit time distributions and transport: Theory and application to storage-dependent transport of chloride in a watershed, Water Resources Research, 51, 1–30, 2015.

Hövel, A., Stumpp, C., Bogena, H., Lücke, A., Strauss, P., Blöschl, G., and Stockinger, M.: Repeating patterns in runoff time series: A basis for exploring hydrologic similarity of precipitation and catchment wetness conditions, Journal of Hydrology, 629, 130 585, 2024.

Hrachowitz, M., Savenije, H., Bogaard, T. A., Tetzlaff, D., and Soulsby, C.: What can flux tracking teach us about water age distribution patterns and their temporal dynamics?, Hydrology and Earth System Sciences, 17, 533–564, https://doi.org/10.5194/hess-17-533-2013, 2013.

Hrachowitz, M., Fovet, O., Ruiz, L., Euser, T., Gharari, S., Nijzink, R., Freer, J., Savenije, H., and Gascuel-Odoux, C.: Process consistency in models: The importance of system signatures, expert knowledge, and process complexity, Water resources research, 50, 7445–7469, 2014.

Hrachowitz, M., Fovet, O., Ruiz, L., and Savenije, H. H.: Transit time distributions, legacy contamination and variability in biogeochemical 1/fα scaling: How are hydrological response dynamics linked to water quality at the catchment scale?, Hydrological Processes, 29, 5241–5256, https://doi.org/10.1002/hyp.10546, 2015.

Hrachowitz, M., Benettin, P., Breukelen, B. M. V., Fovet, O., Howden, N. J. K., Ruiz, L., Velde, Y. V. D., and Wade, A. J.: Transit times—The link between hydrology and water quality at the catchment scale, Wiley Interdisciplinary Reviews: Water, 3, 629–657, 2016.

Hrachowitz, M., Stockinger, M., Coenders-Gerrits, M., Ent, R., Bogena, H., Lücke, A., and Stumpp, C.: Reduction of vegetation-accessible water storage capacity after deforestation affects catchment travel time distributions and increases young water fractions in a headwater catchment, Hydrology and Earth System Sciences, 25, 4887–4915, https://doi.org/10.5194/hess-25-4887-2021, 2021.

Janos, D., Molson, J., and Lefebvre, R.: Regional groundwater flow dynamics and residence times in Chaudière-Appalaches, Québec, Canada: insights from numerical simulations, Canadian Water Resources Journal/Revue canadienne des ressources hydriques, 43, 214–239, 2018.

Jothityangkoon, C., Sivapalan, M., and Farmer, D.: Process controls of water balance variability in a large semi-arid catchment: downward approach to hydrological model development, Journal of hydrology, 254, 174–198, 2001.

Kaandorp, V. P., de Louw, P. G. B., van der Velde, Y., and Broers, H. P.: Transient Groundwater Travel Time Distributions and Age-Ranked Storage-Discharge Relationships of Three Lowland Catchments, Water Resources Research, 54, 4519–4536, https://doi.org/10.1029/2017wr022461, 2018a.

Kaandorp, V. P., Molina-Navarro, E., Andersen, H. E., Bloomfield, J. P., Kuijper, M. J., and de Louw, P. G.: A conceptual model for the analysis of multi-stressors in linked groundwater–surface water systems, Science of the Total Environment, 627, 880–895, 2018b.

Kirchner, J. W., Benettin, P., and van Meerveld, I. V.: Instructive Surprises in the Hydrological Functioning of Landscapes, https://doi.org/10.1146/annurev-earth-071822, 2023.

Klaus, J., Zehe, E., Elsner, M., Külls, C., and McDonnell, J.: Macropore flow of old water revisited: experimental insights from a tile-drained hillslope, Hydrology and Earth System Sciences, 17, 103–118, 2013.

Knighton, J., Souter-Kline, V., Volkmann, T., Troch, P. A., Kim, M., Harman, C. J., Morris, C., Buchanan, B., and Walter, M. T.: Seasonal and topographic variations in ecohydrological separation within a small, temperate, snow-influenced catchment, Water Resources Research, 55, 6417–6435, 2019.

Kuppel, S., Tetzlaff, D., Maneta, M. P., and Soulsby, C.: EcH2O-iso 1.0: Water isotopes and age tracking in a process-based, distributed ecohydrological model, Geoscientific Model Development, 11, 3045–3069, https://doi.org/10.5194/gmd-11-3045-2018, 2018.

Loritz, R., Hassler, S. K., Jackisch, C., Allroggen, N., Van Schaik, L., Wienhöfer, J., and Zehe, E.: Picturing and modeling catchments by representative hillslopes, Hydrology and Earth System Sciences, 21, 1225–1249, 2017.

Maxwell, R. M., Condon, L. E., Kollet, S. J., Maher, K., Haggerty, R., and Forrester, M. M.: The imprint of climate and geology on the residence times of groundwater, Geophysical Research Letters, 43, 701–708, 2016.

McGuire, K. J. and McDonnell, J. J.: A review and evaluation of catchment transit time modeling, Journal of Hydrology, 330, 543–563, 2006.

McMillan, H., Tetzlaff, D., Clark, M., and Soulsby, C.: Do time-variable tracers aid the evaluation of hydrological model structure? A multimodel approach, Water Resources Research, 48, 2012.

Nash, J. E. and Sutcliffe, J. V.: River flow forecasting through conceptual models part I—A discussion of principles, Journal of hydrology, 10, 282–290, 1970.

Pavlin, L., Széles, B., Strauss, P., Blaschke, A. P., and Blöschl, G.: Event and seasonal hydrologic connectivity patterns in an agricultural headwater catchment, Hydrology and Earth System Sciences, 25, 2327–2352, https://doi.org/10.5194/hess-25-2327-2021, 2021.

Rinaldo, A., Benettin, P., Harman, C. J., Hrachowitz, M., McGuire, K. J., van der Velde, Y., Bertuzzo, E., and Botter, G.: Storage selection functions: A coherent framework for quantifying how catchments store and release water and solutes, Water Resources Research, 51, 4840–4847, 2015.

Salmon-Monviola, J., Fovet, O., and Hrachowitz, M.: Improving the hydrological consistency of a process-based solute-transport model by simultaneous calibration of streamflow and stream concentrations, Hydrology and Earth System Sciences, 29, 127–158, 2025.

Sprenger, M., Leistert, H., Gimbel, K., and Weiler, M.: Illuminating hydrological processes at the soil-vegetation-atmosphere interface with water stable isotopes, Reviews of Geophysics, 54, 674–704, 2016.

Stewart, M. K. and Morgenstern, U.: Importance of tritium-based transit times in hydrological systems, Wiley Interdisciplinary Reviews: Water, 3, 145–154, 2016.

Stockinger, M. P., Bogena, H. R., Lücke, A., Diekkrüger, B., Weiler, M., and Vereecken, H.: Seasonal soil moisture patterns: Controlling transit time distributions in a forested headwater catchment, Water Resources Research, 50, 5270–5289, 2014.

Stockinger, M. P., Bogena, H. R., Lücke, A., Diekkrüger, B., Cornelissen, T., and Vereecken, H.: Tracer sampling frequency influences estimates of young water fraction and streamwater transit time distribution, Journal of hydrology, 541, 952–964, 2016.

Stockinger, M. P., Bogena, H. R., Lücke, A., Stumpp, C., and Vereecken, H.: Time variability and uncertainty in the fraction of young water in a small headwater catchment, Hydrology and Earth System Sciences, 23, 4333–4347, https://doi.org/10.5194/hess-23-4333-2019, 2019.

Storn, R. and Price, K.: Differential evolution–a simple and efficient heuristic for global optimization over continuous spaces, Journal of global optimization, 11, 341–359, 1997.

Széles, B., Parajka, J., Hogan, P., Silasari, R., Pavlin, L., Strauss, P., and Blöschl, G.: The Added Value of Different Data Types for Calibrating and Testing a Hydrologic Model in a Small Catchment, Water Resources Research, 56, https://doi.org/10.1029/2019WR026153, 2020.

Türk, H., Stumpp, C., Hrachowitz, M., Schulz, K., Strauss, P., Blöschl, G., and Stockinger, M.: Soil moisture and precipitation intensity control the transit time distribution of quick flow in a flashy headwater catchment, Hydrology and Earth System Sciences Discussions, 2024, 1–33, 2024.

van der Velde, Y., Rozemeijer, J. C., De Rooij, G. H., van Geer, F. C., Torfs, P. J. J. F., and de Louw, P. G. B.: Improving catchment discharge predictions by inferring flow route contributions from a nested-scale monitoring and model setup, Hydrology and Earth System Sciences, 15, 913–930, https://doi.org/10.5194/hess-15-913-2011, 2011.

van der Velde, Y., Torfs, P. J. J. F., van der Zee, S. E. A. T. M., and Uijlenhoet, R.: Quantifying catchment-scale mixing and its effect on time-varying travel time distributions, Water Resources Research, 48, https://doi.org/10.1029/2011WR011310, 2012.

van der Velde, Y., Heidbüchel, I., Lyon, S., Nyberg, L., Rodhe, A., Bishop, K., and Troch, P.: Consequences of mixing assumptions for time-variable travel time distributions, Hydrological Processes, 29, 3460–3474, https://doi.org/10.1002/hyp.10372, 2015.

Visser, A., Heerdink, R., Broers, H., and Bierkens, M.: Travel time distributions derived from particle tracking in models containing weak sinks, Groundwater, 47, 237–245, 2009.

Vreugdenhil, M., Széles, B., Wagner, W., Strauß, P., Oismueller, M., Parajka, J., Blöschl, G., and Hogan, P.: Non-linearity in event runoff generation in a small agricultural catchment, Hydrological Processes, pp. 1–16, https://doi.org/10.1002/hyp.14667, 2022.

Wang, S., Hrachowitz, M., Schoups, G., and Stumpp, C.: Stable water isotopes and tritium tracers tell the same tale: no evidence for underestimation of catchment transit times inferred by stable isotopes in StorAge Selection (SAS)-function models, Hydrology and Earth System Sciences, 27, 3083–3114, 2023.

Wang, S., Hrachowitz, M., Schoups, G., and Störiko, A.: Multi-decadal stability of water ages and tracer transport in a temperate-humid river basin, Environmental Research Letters, 2025.

Weiler, M., McGlynn, B. L., McGuire, K. J., and McDonnell, J. J.: How does rainfall become runoff? A combined tracer and runoff transfer function approach, Water Resources Research, 39, https://doi.org/10.1029/2003WR002331, 2003.

Wiekenkamp, I., Huisman, J. A., Bogena, H. R., Graf, A., Lin, H. S., Drüe, C., and Vereecken, H.: Changes in measured spatiotemporal patterns of hydrological response after partial deforestation in a headwater catchment, Journal of Hydrology, 542, 648–661, 2016.

Yadav, M., Wagener, T., and Gupta, H.: Regionalization of constraints on expected watershed response behavior for improved predictions in ungauged basins, Advances in water resources, 30, 1756–1774, 2007.

Zehe, E., Lee, H., and Sivapalan, M.: Dynamical process upscaling for deriving catchment scale state variables and constitutive relations for meso-scale process models, Hydrology and Earth System Sciences, 10, 981–996, 2006.

Zehe, E., Loritz, R., Edery, Y., and Berkowitz, B.: Preferential pathways for fluid and solutes in heterogeneous groundwater systems: self-organization, entropy, work, Hydrology and earth system sciences, 25, 5337–5353, 2021.

Zuber, A.: On the interpretation of tracer data in variable flow systems, Journal of Hydrology, 86, 45–57, 1986.